Artificial Intelligence Research and Applications (AIra)
https://www.ijaira.org/ Online ISSN: 3108-3889
H. Gasmi et al., Vol. 2, No. 2, June, 2026 Research Article

Mitigating Power Oscillations in DPIG Wind Turbines via Particle-Swarm-Optimized Fractional-Order PI Control

Hamza Gasmi *‡, Habib Benbouhenni **, Tahar Tafticht *, Nicu Bizon ***

* Université du Québec en Abitibi-Témiscamingue, Department of Engineering, Canada.

** Ecole Nationale Polytechnique d'Oran, Laboratoire LAAS, Bp 1523 EL M'NAOUER, Oran, Algeria.

*** The National University of Science and Technology Politehnica Bucharest, Pitești University Centre, Pitesti, Romania.

(hamza.gasmi@uqat.ca, habib.benbouhenni@enp-oran.dz, tahar.tafticht@uqat.ca, nicu.bizon1402@upb.ro)

‡ Corresponding Author: Hamza Gasmi, Université du Québec en Abitibi-Témiscamingue, Department of Engineering, Canada, hamza.gasmi@uqat.ca.

Received: 12.10.2025, Revised: 22.01.2026, Accepted: 27.03.2026

Abstract- This study improves the field-oriented control (FOC) strategy used in double-powered induction generator (DPIG) wind-turbine systems by replacing traditional proportional–integral (PI) controllers with fractional-order PI regulators tuned through particle swarm optimization (FOPI-PSO). The proposed FOC–FOPI-PSO framework integrates three optimized controllers that enhance energy extraction and stabilize the power delivered to the grid. In contrast to previous PSO-based fractional or hybrid control approaches—which often add computational burden or focus on different machine configurations—this work embeds a PSO-tuned fractional PI controller directly into the standard FOC architecture of a DPIG. This preserves the simplicity of conventional PI implementation while specifically improving DPIG power-flow behavior, delivering quicker transient response and substantially attenuated power oscillations. MATLAB simulations demonstrate marked performance gains: active-power oscillations are reduced by 90.90%, response time improves by 2.52%, and steady-state error drops by 89.09% relative to traditional FOC–PI control. Additionally, current total harmonic distortion decreases by approximately 99.46%. These results highlight the proposed method as a highly effective and reliable control solution for modern wind-energy systems.

Keywords: Double-powered induction generator, fractional-order PI controller, wind turbine system, particle swarm optimization, maximum power energy.

1. Introduction

The worldwide worry about the increasing consumption of electrical power (EP), environmental pollution, and the possible depletion of fossil fuels has prompted a growing interest in renewable energies (REs), especially after the Paris Agreement adopted by 196 parties at COP 21 in Paris [1]. Global warming is among the most important phenomena that have affected nature greatly as a result of the increased and excessive use of fossil energies to generate EP, as the use of these traditional energies leads to the spread of toxic gases. The latter affects the lives of humans and animals greatly,

Cite this article as: H. Gasmi, H. Benbouhenni, T. Tafticht, and N. Bizon, "Mitigating Power Oscillations in DPIG Wind Turbines via Particle-Swarm-Optimized Fractional-Order PI Control," *Artificial Intelligence Research and Applications (AIra)*, Vol. 2, No. 2, pp. 103–123, June, 2026, https://doi.org/10.20508/816jem12.

which led scientists to search for other alternatives to fossil energies. Accordingly, nature has resorted to a large extent to generate EP, by relying on endless natural forces such as wave energy, solar energy, and wind power (WP). These energies are called REs, as they are clean, non-polluting, and do not pose a threat to the environment. On the contrary, it is among the energies that help the environment and protect it from toxic gas emissions.

Among various RE sources, WP is regarded as one of the most promising RE resources in the world. Globally, there are several structures of WP conversion systems (WPCSs), which can be generically classified into two large groups: constant-speed power conversion systems [2] and variable-speed WPCS [3]. Several types of generators are used to generate electricity from the wind, such as the induction generator (IG) [4], the synchronous generator [5], DC generators [6], and doubly-fed IGs (DFIGs) [7]. In addition to generators, transformers, and inverters are used. The latter is used to regulate the power generated by electric generators.

Nowadays, WECS using double powered induction generator (DPIG) is the most preferable configuration for WECS installed or under construction because of its remarkable advantages. The DPIG allows active (*Ps*) and reactive power (*Qs*) control, minimization of mechanical stress and noise, good overall effectiveness, and low rating converter [8].

To control the generator, several control schemes are used, such as linear controls, hybrid controls, intelligent controls, and nonlinear controls. Linear strategies are among the strategies whose simplicity and ease of application are two of the biggest positives, as these strategies can be applied to complex systems easily [9]. Moreover, these strategies are inexpensive and the systems controlled by these strategies can be maintained at a lower cost. Linear strategies are represented by both direct torque control (DTC) [10] and direct power control (DPC) [11]. In DPC/DTC, Reference values are controlled by hysteresis comparators (HCs), and the rotor side converter (RSC) is regulated using a switching table (ST). The main disadvantage of these strategies is that they contain large ripples in different variables such as torque and electric current [12]. On the other hand, numerous nonlinear control laws such as sliding mode control (SMC) [13], synergetic control (SC) [14], predictive control [15], backstepping control (BC) [16], high-order SMC technique [17-19], fractional-order control [20], and passivity control [21], have been presented in many works.

The main objective of these control techniques is to improve the robustness against parameter variations and model uncertainty. So, these nonlinear controls are characterized by high durability compared to linear controls, because they are not affected much by changing the generator parameters, which recommends them as the best solutions in the field of control. However, their disadvantage is that they are complex, difficult to realize, and depend on the MM (mathematical model) of the machine.

Similar in performance to nonlinear control schemes are intelligent controls such as FL (Fuzzy Logic) and NNs (Neural Networks) that provide better results in terms of enhancing the competence and speed of dynamic response (DR) to machines [22-24]. In [25], the FL is used to enhance the efficiency and features of the DTC of the AG-based wind turbine system (WTS). The results showed the performance of the FL approach in improving the current quality and minimizing the response time (RT) of the *Ps* and *Qs*. In [26], the author gave a novel idea for the DPC by using NNs algorithms, where the ST is removed and replaced by NN to minimize the *Qs* and *Ps* ripples and improve the current quality of the generators. By seeing the results, it can be said that NNs are one of the best solutions that can be suggested to control generators.

Another smart control was used in [27] to improve the behavior of the DPC, where the GA (Genetic Algorithm) was used to improve the efficiency of the DPC based on the modified space vector modulation (SVM). The numerical results showed that the PI-GA is better than the PI regulator in several aspects such as minimizing the fluctuations of both the torque, *Ps*, and the current. Also, underestimate the current THD (Total Harmonic Distortion). FL and GA were combined to improve the features of the DFIG [28]. The combination of the two approaches leads to a significant minimization in energy ripples, with a higher current quality compared to the DPC.

In [29], a particle swarm optimization-based PI (PI-PSO) was designed to regulate the *Qs* and *Ps* of the DFIG. The results showed that the PI-PSO is more efficient and performant than the PI and this is shown by the RT, energy ripples, and current THD. In [30], both GA and PSO were used to determine the parameters of the P and PI, where these two intelligent controllers are used to control the energy for 9 MW DFIG. Through the simulation results performed, it is revealed that the PSO-based regulators perform better compared to both the classical regulators and the GA-based techniques. On the other hand, the PSO is applied to optimize the distribution of *Qs* among groups [31], where the designed technique greatly minimizes the number of variables for optimization and increases the calculation speed of the technique.

In [32], a wind speed (WS) estimation scheme for a DFIG-WTS is designed, in which a new OPSO-SVR is introduced to estimate the WS value based on the training data from the previous offline training. In [33], a new strategy for designing the control system of a DFIG-based dish-stirling system is designed to achieve maximum power point tracking (MPPT) and constant receiver temperature regulation, whereby the PSO is used to estimate the parameters of the suggested system.

The use of linear controls, nonlinear controls, or smart controls in controlling electrical machines, especially generators, is not sufficient, as the cons of ripples remain at the level of *Ps*, torque, and current, with a reduction in the current quality, and this is undesirable in the area of control. Therefore, scientists resorted to new strategies under the name of hybrid control, where two or several controls are combined to achieve a more robust and efficient strategy for electric machine control. The idea of fusion (or merger) has recently emerged as an alternative solution to linear and non-linear strategies, whereby two controls that are different in principle

but similar in control idea can be combined. In [34], the author combined SC and STC (super-twisting control) to control the DFIG energy, where the combination of the two nonlinear strategies resulted in a significant enhancement in the current quality compared to the usual control. Also, the obtained control is characterized by ease of realization and simplicity, where durability is among the most important features obtained from this merger.

In [35], the SMC technique and SC were combined, and the obtained strategy was named SC-SMC. In this new approach, the author has omitted a continuous part of SMC and replaced it with a SC technique, where simplicity and robustness are two of the major positives of this new nonlinear control. The results proved the efficiency of the designed control in minimizing the *Qs* and *Ps* fluctuations, and this appears in the very high minimization ratios compared to the classical control. Two nonlinear methods have been combined in [36] represented by the SMC technique and BC for controlling DFIG. The results proved the efficiency of the control obtained from the merger in enhancing the features of the generator compared to the classical approach. But the cons of this approach are the complexity and difficulty of achievement. Also, this designed strategy is costly and cannot be easily applied to complex systems.

Another merger between two different methods was done in [37-39], which in this case are the fractional-order control and the PSO. These two controls were used to increase the effectiveness of the PI of *Qs* and *Ps* of the DFIG. The designed technique is described by ease of application and high robustness compared to the DPC. However, the disadvantage of this control is the use of the PSO, as this program takes a lot of time to calculate the fractional-order PI parameters. In [40], NNs and STC were combined to improve the characteristics of the DPC of DFIG through the NN-STC controller which replaced the traditional HC. In addition, a modified SVM was used in place of the ST, and it was noted that the robustness of the DPC was significantly increased in the case of using a NN-STC controller.

SMC technique was combined with NNs [41], FL [42], and neuro-FL [43] to control the WTS, where the use of smart approaches led to a significant augment in the robustness of the SMC technique while ameliorating the current network quality compared to classical techniques. In [44], three approaches were combined to control the WP generation system using DFIG, and these approaches are DPC, SMC, and PSO algorithms. On the other hand, the NN algorithms have been used to estimate WS. Results showed that the designed technique is more robust than the usual approach. In [45], a 2 MW DFIG was controlled using the combination of vector controls and two different DPC techniques. The designed technique is verified under normal, unbalanced, and distorted voltage conditions. Three smart approaches were compared, as these approaches are direct virtual torque control, DPC approach, and voltage-oriented control [46].

These proposed approaches are based on the NN algorithm and the comparison was made in terms of the potential ripple ratio, RT, and current quality. The results on a 4000 W generator are explained using MATLAB together with the NN Toolbox. Results showed that the DPC-NN is the best in terms of ripples and current quality. Experimental results on a DPC-controlled 2 KW DFIG prototype based on the SMC technique are presented [47]. The results of the experiment demonstrated the competence of the combination of the two approaches by improving the quality of the electric current and the DFIG characteristics. A combination of DPC approach and STC is designed to control 2 MW DFIG under unbalanced and balanced grid voltage conditions [48]. The use of the STC significantly improves the characteristics of the DPC and improves the network's current quality compared to the DPC. In [49], the STC controller associated with the FL control to realize optimal control performance of the WTS-based DFIG. However, the DPC using an FL-STC is compared with the usual method in terms of tracking references, undershoot, current THD, and steady-state error (SSE). The suggested control is efficient in minimizing the power ripples; successfully suppressing the chattering problem and the effects of parametric variations (which no longer affect the tuning competence).

The combination of approaches leads to a significant enhancement in current quality while minimizing *Ps* and *Qs* ripples. However, on the other hand, it increases system complexity, cost, and implementation difficulty, and this is not desirable. In general, the combination of approaches is among the best solutions that can be suggested for regulating generators, especially in the field of REs in general.

In this work, a new strategy described by robustness, ease of application and simplicity is put forward to control the capacities of the DPIG-based WTS. This control is represented by the combination of PI, fractional calculus, and PSO to obtain a more efficient strategy that has the high ability to improve the robustness of traditional controls. First, the fractional-order control is implemented on the PI to increase its capabilities and efficiency of the PI. Second, the PSO is used to calculate the parameters of the fractional-order PI (FOPI). The FOPI based on the PSO is designed as the best solution in this paper because of its ease of setup, tuning, and implementation.

The contribution of the paper lies in the use of a FOPI-PSO in improving the efficiency and characteristics of the indirect FOC (IFOC), where four FOPI-PSO regulators are used to control the *Qs* and *Ps* of the DPIG-based WTS. Also, FOPI-PSO is used to optimize the MPPT to obtain the largest value of the ME generated from WP. Compared to the FOPI-PSO, PI has a medium degree of complexity. However, it is described by very high robustness compared to both hysteresis and PI controllers, and this is shown by the ripple minimization ratio of *Ps* and *Qs*, current quality, values of each of the overshoot, and SSE errors.

While previous studies such as [37], [38], and [44] have explored hybrid control strategies—including PSO-tuned fractional schemes and intelligent PI variants—these methods typically introduce additional structural complexity, rely on auxiliary compensators, or are designed for machine types other than DPIG systems. In contrast, the originality of this work lies in embedding a PSO-optimized fractional-order PI (FOPI-PSO) controller directly within the standard field-

oriented control (FOC) loops of a double-powered induction generator, without modifying the core FOC architecture or adding supplementary control layers. This yields a controller that maintains the implementation simplicity and computational lightness of a classical PI, while providing the enhanced tuning flexibility and robustness of fractional calculus.

Moreover, unlike earlier hybrid approaches that primarily enhance transient performance, the proposed method delivers simultaneous improvements across multiple performance indices. Specifically, it achieves a 99.46% reduction in current THD, a 90.90% decrease in active-power oscillations, an 89.09% reduction in steady-state error, and a 2.52% faster dynamic response. This combination of simplicity, broad-spectrum performance enhancement, and direct applicability to DPIG-based wind-energy systems constitute a novel and practical contribution to advanced renewable-energy control.

The approach developed in this paper was validated in a MATLAB environment using a 1500 kW generator. Furthermore, variable wind speed was employed to study the effectiveness and efficiency of this approach in improving power and current quality.

The goals achieved in this work are: (1) Reducing ripples in the *Qs*, torque, current, and *Ps*; (2) Providing an easy and less complex control scheme to be used to control complex systems; (3) Improving the current THD; (4) Increasing the robustness of the controlled generator; (5) Improving the characteristics of the conventional IFOC; (6) Giving a new scheme to a more robust FOPI controller.

A comparative study has been conducted in several respects between the suggested control and the FOC. Also, a comparative study was carried out between the completed study and published papers in terms of the value of the current THD and the undulation minimization ratio of the *Qs* and *Ps*. Figure 1 represents the proposed work in this paper, where a comparative study is done at the end of the paper.

The paper is prepared as follows. The modelling of the WTS is given in section 2. The FOPI-PSO is dedicated in section 3. The conventional IFOC of the DPIG-based WTS is explained in section 4. Section 5 describes the IFOC technique based on the designed FOPI-PSO controller of the RSC. In section 6, results are shown and discussed. The work's conclusions are presented in section 7.

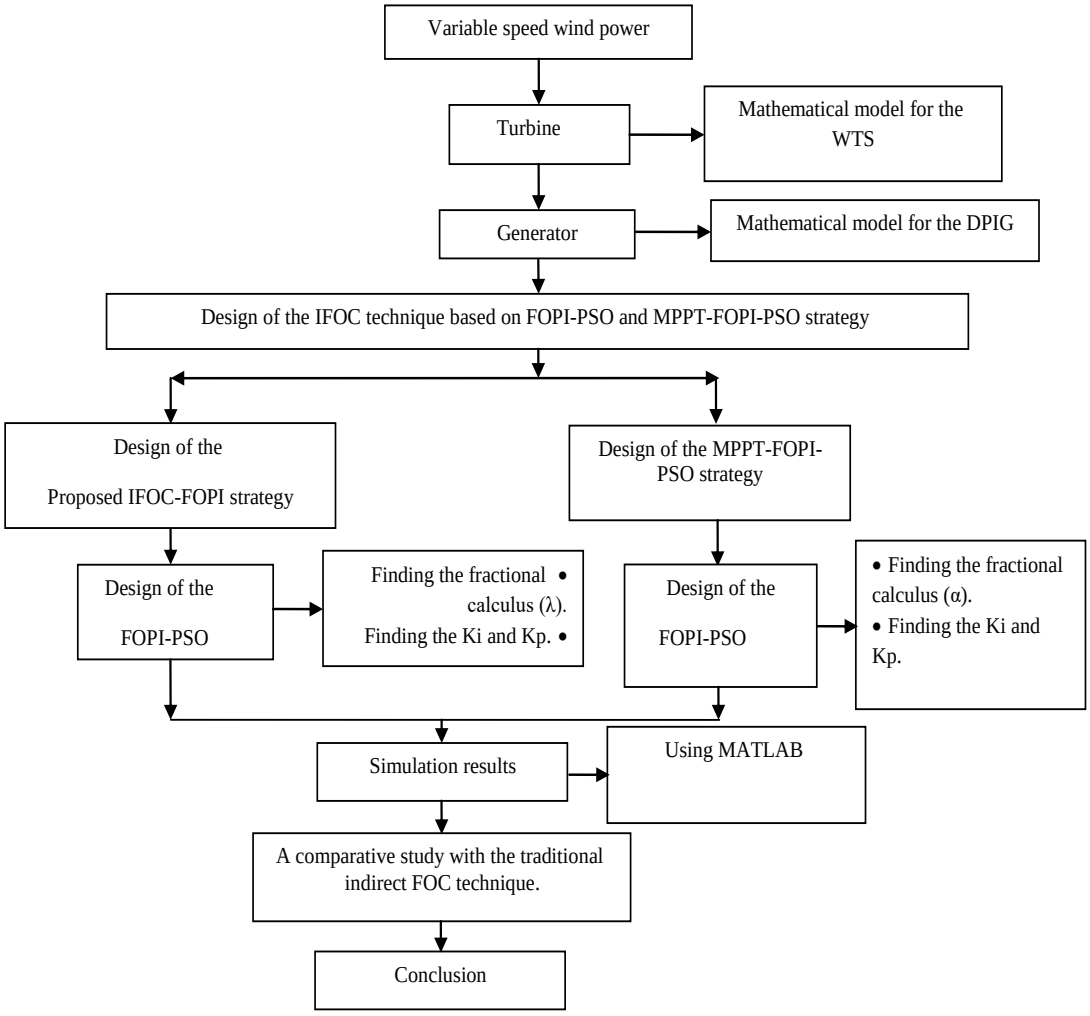

Fig. 1. Stages of implementing the proposed strategy.

2. WTS Model

The system of generating EP from WP is among the systems that have known great development and widespread use in recent years due to the non-emission of toxic gases its preservation of the environment and the reduction of the use of traditional sources of energy. The WTS can be represented as in Figure 2, where simplicity, ease of implementation, and low charge of realization are among the biggest positives of this system. Through this figure, and in order to generate EP from wind, both WTs and electric generators are used. Also, the two inverters are used to feed the DPIG. The feature of this system is that several types of WTs can be used, such as multi-rotor WTs [50] and single-rotor WTs [51]. In addition to WTs, several electric generators can be used, but DPIG remains one of the most excellent solutions that can be suggested in the case of variable WSs.

The output energy of the WT can be articulated by the following equation [52]:

$$P_t = 0.5\rho\pi R^2 C_p(\lambda,\beta)V^3 \tag{1}$$

where, ρ is the air density, V is the WS, R is the blade length, and Cp is the power coefficient which is generally expressed as a function of the λ (tip speed ratio) and the β (pitch angle). For a 1.5 MW turbine, the Cp can be modelled by [53]:

$$C_p(\lambda,\beta) = \frac{46}{100}\left(\frac{151}{\lambda_i} - \frac{58}{100}\beta - \frac{2}{1000}\beta^{2.14} - 13.2\right)e^{\frac{-18.4}{\lambda_i}} \tag{2}$$

$$\lambda_i = \frac{1}{\lambda + 0.02\beta} - \frac{0.003}{\beta^3 + 1} \tag{3}$$

The λ is given by Equation (4).

$$\lambda = \frac{R\Omega_t}{V} \tag{4}$$

The WT is generally connected to the DPIG shaft through a gearbox system whose transmission ratio G is chosen so that the speed of the DPIG shaft Ω_{mec} remains within the desired speed range.

If we neglect the elasticity, friction, and power losses in the gearbox, the torque T_g and speed Ω_{mec} of the generator shaft side can be given, as a function of the WT speed Ω_t and torque T_t, by the following equations [54]:

$$\begin{cases} T_g = \dfrac{T_t}{G} = \dfrac{P_t}{G\Omega_t} \\ \Omega_{mec} = G\Omega_t \end{cases} \tag{5}$$

The fundamental equation of dynamics can be written as follows:

$$J_{tot}\frac{d\Omega_{mec}}{dt} = T_g - T_{em} - f\Omega_{mec} \tag{6}$$

Where, T_{em} is the torque generated by DPIG and J_{tot} is the complete friction coefficient.

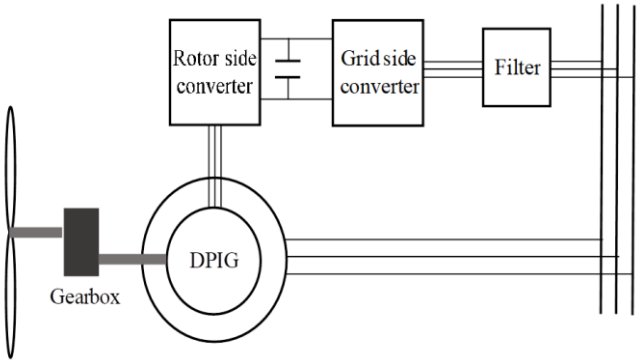

Fig. 2. Scheme of the studied WTS.

The second element that is of great importance in the WTS is the generator, as this generator is the cornerstone for producing EP from the WP. The DPIG converts the mechanical power gained from the WP by the turbine into electrical energy.

In this work, a DPIG-type generator is used due to the simplicity of control and robustness compared to other kinds. The Park transform is used to give the MM of this machine, where this form is shown in the equations from Equation (7) to Equation (14) [55]. Equation (7) represents the stator and rotor voltage of the DPIG.

$$\begin{cases} V_{qs} = R_s I_{qs} + w_s\varphi_{ds} + \dfrac{d\varphi_{qs}}{dt} \\ V_{ds} = R_s I_{ds} - w_s\varphi_{qs} + \dfrac{d\varphi_{ds}}{dt} \\ V_{qr} = R_r I_{qr} + (w_s - w_r)\varphi_{dr} + \dfrac{d\varphi_{qr}}{dt} \\ V_{dr} = R_r I_{dr} + \dfrac{d\varphi_{dr}}{dt} - \varphi_{qr}(w_s - w_r) \end{cases} \tag{7}$$

The flux equations are expressed as:

$$\begin{cases} \varphi_{ds} = I_{ds}L_s + I_{dr}M \\ \varphi_{qs} = I_{qr}M + I_{qs}L_s \\ \varphi_{dr} = I_{dr}L_r + I_{ds}M \\ \varphi_{qr} = I_{qr}L_r + I_{qs}M \end{cases} \tag{8}$$

The Qs and Ps can be defined as follows [56]:

$$\begin{cases} P_s = I_{ds}V_{ds} + I_{qs}V_{qs} \\ Q_s = I_{ds}V_{qs} - I_{qs}V_{ds} \end{cases} \tag{9}$$

To make an independent control of the Qs and Ps, the quadrature component of the stator flux is set to zero by the orientation of the direct axis in the direction of the stator flux.

$$\begin{cases} \varphi_{ds} = \varphi_s \\ \varphi_{qs} = 0 \end{cases} \tag{10}$$

By ignoring the resistances of the stator phases, Equation (11) represents the stator voltage [57].

$$\begin{cases} V_{ds} = 0 \\ V_s = V_{qs} = w_s \varphi_s \end{cases} \quad (11)$$

The *Qs* and *Ps* equations can be simplified as:

$$\begin{cases} P_s = -\dfrac{M}{L_s} V_s I_{qr} \\ Q_s = -\dfrac{M}{L_s} V_s I_{dr} + \dfrac{V_s^2}{w_s L_s} \end{cases} \quad (12)$$

Equation (13) represents the rotor voltage of the machine.

$$\begin{cases} V_{dr} = I_{dr} R_r + \sigma L_r \dfrac{dI_{dr}}{dt} - \sigma L_r w_r I_{qr} \\ V_{qr} = R_r I_{qr} + \sigma L_r \dfrac{dI_{qr}}{dt} + A \end{cases} \quad (13)$$

with:

$$A = \sigma L_r w_r I_{dr} + w_r g \frac{M}{L_s} \varphi_s$$
$$\sigma = 1 - \frac{M^2}{L_r L_s} \quad (14)$$

3. Proposed FOPI-PSO Controller

One of the most popular controllers used so far is the PI controller. This type is identified by ease of application and simplicity compared to many other regulators such as SMC and BC regulators. Also, the PI has the advantage of being more stable. But its use in electrical systems creates several problems and the desired results are not obtained. The use of this kind of regulator leads to a rather slow DR compared to some recently developed control strategies. In addition, the use of a PI causes the studied WTS to be affected by changing parameters and this is undesirable. On the other hand, PI controllers may not be sufficient to deal with complex systems.

There are several solutions suggested to enhance the robustness and competence of the PI derivative (PID), especially by intelligence controls such as FL [58], NN algorithm [59], PSO strategy [60], and genetic algorithms [61]. For better performance, a fractional calculus was introduced as an alternative to the PID.

Fractional-order control is a mathematical method designed to significantly improve the efficiency of systems, as it provides superior results in terms of DR compared to conventional controls. This control has been used in many different fields.

Using fractional calculus will increase the efficiency and robustness of the PID. The expression of the PID based on fractional-order control ($PI^{\delta}D^{\mu}$) in the time domain is described as follows [62]:

$$u(t) = K_p e(t) + K_i D^{-\delta} e(t) + K_d D^{\mu} e(t) \quad (15)$$

Where, K_d is the derivative constant gain, e(t) is the error signal, K_p is the proportional constant gain, u(t) is the control signal, K_i is the integration constant gain, δ and μ are the non-integer orders of the integral and derivative terms, respectively.

D^{α} is a generalized fractional integral/derivative operator of fractional-order α. The most commonly encountered definition of the fractional operator is called the Riemann-Liouville description, in which the fractional operator is defined as follows [63]:

$${}_a D_t^{\alpha} f(t) = \frac{1}{\Gamma(n-\alpha)} \frac{d^n}{dt^n} \left[\int_a^t \frac{f(\tau)}{(t-\tau)^{\alpha-n+1}} d\tau \right] \quad (16)$$

where, $\Gamma(.)$ is Euler's gamma function, n is an integer which satisfies the condition $n - 1 < \alpha < n$, a and t are the limits of integration. The Laplace transform of the Equation (16) under zero initial conditions is given by the following equation:

$$L\left\{ {}_a D_t^{\alpha} f(t) \right\} = \int_0^{\infty} e^{-st} {}_a D_t^{\alpha} f(t) dt = s^{\alpha} F(s) \quad (17)$$

Equation (15) can be written according to Equation (18).

$$G(s) = \frac{U(s)}{E(s)} = K_p + K_i s^{-\delta} + K_d s^{\mu} \quad (18)$$

In this work, we have chosen a FOPI structure, with K_d = 0, which is a general form of the PI. The main feature of the FOPI controller is the fact that it has an additional tuning parameter (integral order α) which can be used to improve the efficiency of the control loop.

Accordingly, the MM of the FOPI used in this paper is shown in Equation (19). Also, Equation (20) represents the proposed and used control unit function to improve the efficiency and characteristics of the FOPI [64].

$$u(t) = K_i D^{-\delta} e(t) + K_p e(t) \quad (19)$$

$$G(s) = \frac{U(s)}{E(s)} = K_p + K_i s^{-\delta} \quad (20)$$

Through equation (19), it is noted that the designed control is simple, uncomplicated, inexpensive, and easy to perform. In addition, it can be easily programmed compared to other controllers like SMC or BC. Moreover, this proposed control contains three parameters K_p, K_i, and δ, which makes it easy to adjust. In order to calculate these parameters several strategies can be used such as GA, PSO strategy, grey wolf optimization, etc.

In Figure 3, an illustration of the proposed FOPI controller is given in this work to simplify the understanding. In this unit, there are parameters to be calculated and for their calculation, the PSO is used in this part of the paper.

The PSO was used to produce the FOPI parameters because it is the best strategy in the field, providing better results than several algorithms such as the GA. In addition, it is described by high accuracy and no difficulty of use.

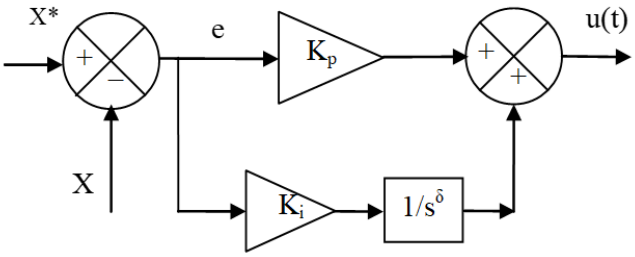

Fig. 3. The FOPI controller.

Traditionally, the PSO is a heuristic search technique that is designed by Kennedy and Eberhart in the mid-1990s [65]. It is based on the simulation of the social behaviour and movement of individual members in a bird flock or fish school searching for food sources. Today, PSO is one of the most widely used algorithms to solve engineering optimization problems. During each iteration in PSO, each particle moves according to its own experiences in the search space, searching for promising regions, while also relying on the experiences of its neighbours in the search process [66].

The initialization procedure lets the swarm particles be randomly dispersed within pre-defined ranges across the search space. The following equation allows the creation of the initial population.

$$x_0^i = x_{\min} + rand\left(x_{\max} - x_{\min}\right) \tag{21}$$

rand is random variable between 0 and 1. x_{max} and x_{min} are upper and lower limits of variables.

The best position of i^{th} particle is named local best position $Pbest_k^i$. However, the entire swarm's best-known position is called global best position $Gbest_k^i$ of the current swarm *k*. The formula for updating the velocity v_i^{k+1} of each particle is given by [67]:

$$v_i^{k+1} = wv_i^k + H) \tag{22}$$

with: $H = c_2 rand(Gbest_i^k - X_i^k) + c_1 rand(Pbest_i^k - X_i^k)$

X_i^k and v_i^k are the position and speed of particle *i* at the previous iteration *k*. *w*, c_1 and c_2 are control parameters, chosen constant or adapted during the iterations.

The position of each particle is updated using its speed as shown in Equation (23).

$$x_i^{k+1} = x_i^k + v_i^{k+1} \tag{23}$$

In this step, the best local positions of all particles and the best global position are memorized for use in the next iteration. For a minimization problem, updating is made by Equations (24) and (25) [68].

$$Pbest_i^k = P_i^k \; if \; f(Pbest_i^k) > P_i^k \tag{24}$$

$$Gbest_i^k = P_i^k \; if \; f(Gbest_i^k) > P_i^k \tag{25}$$

where, *f(x)* it is the fitness function.

The steps of updating speeds (velocities), positions, local best positions, and global best positions are repeated until the desired convergence criterion is reached.

To get the most excellent parameters (K_p, K_i, δ) of the three FOPI regulators used in the two current loops and the MPPT strategy, the integral absolute error (IAE) is used to determine the formulation of the optimization problem, where it is the sum of the absolute errors between the actual values of speed, energies and currents, respectively, and their reference values:

$$IAE = \int_0^{\infty} |e(t)| dt = \int_0^{\infty} \left(\left| I_{qr}^* - I_{qr} \right| + \left| I_{dr}^* - I_{dr} \right| + \left| \Omega_{mec}^* - \Omega_{mec} \right| \right) dt \tag{26}$$

The use of the PSO to improve the behaviour of the FOPI regulator leads to an improvement in the current quality created by the DPIG. It also leads to the reduction of ripples of torque, *Ps*, and current. A simple form can be given by which we illustrate the suggested regulator in this work to improve the robustness of the IFOC. Figure 4 represents the proposed FOPI-PSO to regulate the DPIG power. With this look, the designed intelligent nonlinear controller is simple, uncomplicated, easy to perform, and more durable compared to the classical controller such as an HC or PI controller.

The stability of the FOPI-PSO controller is studied using either the graphical or algebraic method. The graphical method relies on the Bode curve, where curves are derived for both phase and magnitude. Stability is then proven using this method based on the values of margin gain and margin phase. The second method is the algebraic method. This algebraic method relies on Lyapunov's theorem, which is the most common method for proving stability. Therefore, the stability of this system was proven using Lyapunov's theorem. Equation (19) is used to demonstrate this stability.

To demonstrate this stability, the following steps are necessary:

Step 1: Fault dynamics in a closed loop

To facilitate proving stability and calculations, a first-order system is imposed, from which the result can be extended to higher-order systems. Therefore, the Equation (27) can be written as:

$$\dot{e}(t) = -ae(t) + bu(t) \tag{27}$$

With: $a > 0$ and $b > 0$.

Using Equation (19), Equation (27) can be written according to Equation (28).

$$\dot{e}(t) = -(a - bK_p)e(t) + bK_i D^{-\delta} e(t) \tag{28}$$

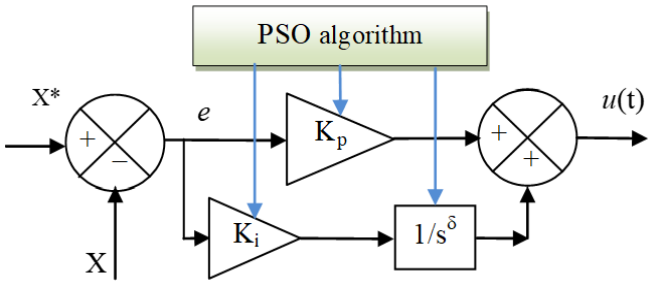

Fig. 4. The FOPI-PSO controller.

The fractional integral is defined by the following equation:

$$Z(t) = D^{-\delta} e(t) \tag{29}$$

Based on Equation (29), Equation (30) can be written.

$$e(t) = D^{-\delta} Z(t) \tag{30}$$

Step 2: Lyapunov candidate function

In this step, the Lyapunov function is chosen to prove the stability.

Equation (31) represents the Lyapunov function used in this paper to prove the stability of the regulator designed herein.

$$V(t) = \frac{1}{2} e^2(t) + \frac{1}{2} \alpha Z^2(t) \tag{31}$$

The function represented by Equation (31) is positive when the condition alpha is positive.

Step 3: Calculating the Differentiation

In this step, the fractional derivative of the Lyapunov function is calculated. This step is crucial for calculating the differentiation to determine the stability condition.

Using the fractional derivative of Caputo and the well-known properties of fractional calculus:

$$\dot{V}(t) = e(t)\dot{e}(t) + Z\alpha D^{-\delta} Z(t) \tag{32}$$

Therefore, the alternative system dynamics can be written according to Equation (33).

$$V^{\cdot}(t) = -(a - bK\_p)\, e\hat{}2 + (\alpha e(t) Z(t) + bK\_i\, eZ) \tag{33}$$

Equation (33) becomes as follows:

$$\dot{V}(t) = -(a - bK_p) e^2(t) + (\alpha + bK_i) e(t) Z(t) \tag{34}$$

Step 4: Stability condition

$$\alpha = -bK_i \tag{35}$$

Based on Equation (35), the derivative of the Lyapunov function can be written according to the following equation:

$$\dot{V}(t) = -(a - bK_p) e^2(t) \tag{36}$$

Equation (36) satisfies the stability condition when both $K_p > \frac{a}{b}$, $K_i > 0$, and $0 < \delta < 1$ are true.

Therefore, we can write the following:

$$\dot{V}(t) \leq 0 \tag{37}$$

According to Lassalle's principle of stability for fractional order systems, the equilibrium can be written according to Equation (38).

$$\begin{cases} e(t) = 0 \\ Z(t) = 0 \end{cases} \tag{38}$$

Therefore, it can be said that the designed approach is asymptotically stable.

4. Traditional IFOC Technique

As is well known, the FOC is among the frequently used controls of controlling machines, as it has been used to control asynchronous motors [69], synchronous motors [70], and generators [71, 72]. Among the advantages of this control is that it is simple, uncomplicated, and can be done easily [73]. This strategy contains inner loops which makes it rather complicated compared to both DPC and DTC. This approach is based on the use of PI controllers and PWM techniques to run the inverter of the electrical machine. This control is of two kinds, the DFOC and the IFOC [74, 75]. In this part, the IFOC is used to control the DFIG because of the characteristics that distinguish them compared to the DFOC. The IFOC has been studied in several works on renewable energies. This control depends on Equation (10) to give the reference values for the rotor voltage (Figure 5).

The expression of the stator currents becomes:

$$\begin{cases} I_{ds} = -\frac{M}{L_s} I_{dr} + \frac{\varphi_s}{L_s} \\ I_{qs} = -\frac{M}{L_s} I_{qr} \end{cases} \tag{39}$$

Equation (40) represents rotor voltages.

$$\begin{cases} V_{dr} = R_r \cdot I_{dr} - w_r \cdot (L_r - \frac{M^2}{L_s}) \cdot I_{qr} \\ V_{qr} = R_r \cdot I_{qr} + w_r \cdot (L_r - \frac{M^2}{L_s}) \cdot I_{dr} + g \cdot \frac{M \cdot V_s}{L_s} \end{cases} \tag{40}$$

Equation (41) represents the rotor flux.

$$\begin{cases} \varphi_{dr} = (L_r - \frac{M^2}{L_s}) I_{dr} + \frac{M \cdot V_S}{L_S \cdot w_S} \\ \varphi_{qr} = (L_r - \frac{M^2}{L_s}) I_{qr} \end{cases} \tag{41}$$

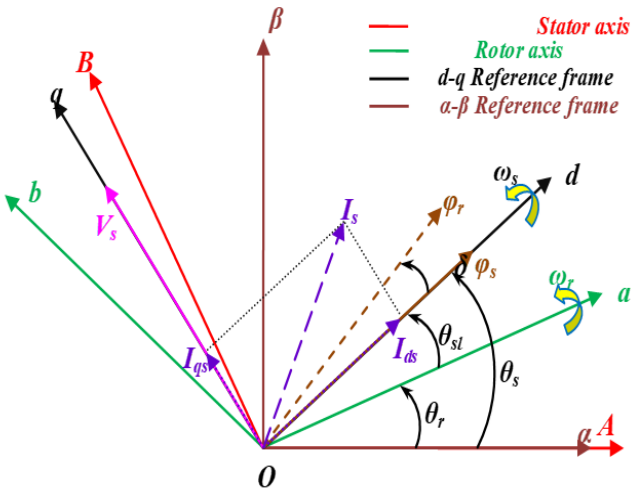

Fig. 5. IFOC method principle.

Equation (42) represents the error in the QRS (quadrature rotor current). Also, the reference of the QRS is shown in Equation (43).

$$e(I_{qr}) = I_{qr}^{*} - I_{qr} \tag{42}$$

$$e(I_{qr}) = I_{qr}^{*} - I_{qr} \tag{43}$$

The direct rotor current of the generator is shown in Equation (44). This current is related to the reference Qs, as shown by Equation (45).

$$e(I_{dr}) = I_{dr}^{*} - I_{dr} \tag{44}$$

$$I_{dr}^{*} = -\frac{L_s}{MV_s} Q_s^{*} + \frac{MV_s}{L_s} \tag{45}$$

Thus, the expressions for both quadrature and direct reference voltage are shown in Equations (46) and (47) respectively. These two equations represent the IFOC-PI, where a traditional PI controller is used to reduce the *Qs* and *Ps* ripples of the DPIG. In this command, two traditional PI regulators are used as shown in Figure 6.

$$V_{qr}^{*} = \left[K_p e(I_{qr}) + K_i \int e(I_{qr})dt\right] + I_{dr} g w_s \sigma + g\frac{MV_s}{L_s} \tag{46}$$

$$V_{dr}^{*} = \left[K_p e(I_{dr}) + K_i \int e(I_{dr})dt\right] - I_{qr} g w_s \sigma \tag{47}$$

The IFOC technique is described by the presence of fluctuations in the level of torque, current, and Ps. Also, slow the DR, as these defects may create problems in the systems and increase regular maintenance. To avoid and reduce these defects, it is suggested to use the FOPI-PSO to improve the characteristics and features of the IFOC. In the next part, the principle of the IFOC-FOPI-PSO and its advantages compared to the IFOC-PI are explained in detail.

5. Proposed FOC-FOPI-PSO Strategy

In this section, a novel nonlinear control is suggested for controlling the DPIG-WTS, which is a change from the IFOC to reduce the ripples of torques, *Ps*, and currents. Also, the DR of both *Qs* and *Ps* is improved. In this suggested control, a new MPPT-FOPI-PSO is used to obtain the reference value of *Ps*. In addition, the reference value of the *Qs* is set at the value 0 VAR. In this IFOC-FOPI-PSO, we need to estimate both the *Qs* and *Ps*, after measuring both current and voltage.

The designed technique is represented in Figure 7, where robustness is among its advantages compared to the IFOC.

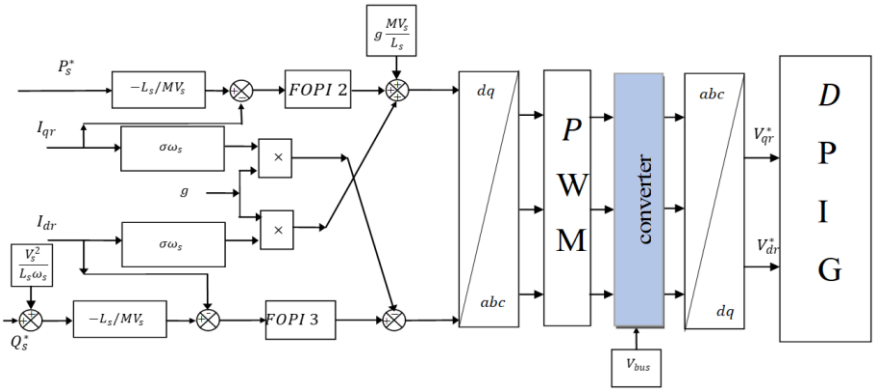

Fig. 6. IFOC technique.

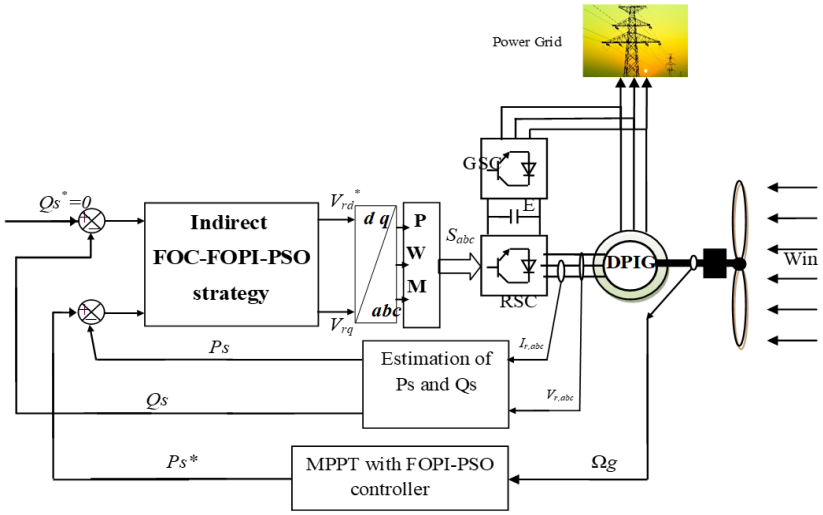

Fig. 7. The block diagram of the designed indirect FOC-FOPI-PSO technique of the DPIG.

Table 1 presents a comparative study between the IFOC-FOPI-PSO and the traditional IFOC-PI in all respects, where the results obtained in this work were relied upon to complete this comparison. It is necessary to give the similarities and differences between the two approaches to clarify the idea of the IFOC-FOPI-PSO using MPPT-FOPI-PSO and its ability to improve the described of the DPIG-WTS as a whole (Table 1). In general, the IFOC-FOPI-PSO using MPPT-FOPI-PSO has many advantages that make it better than the IFOC-PI in terms of the current quality and the rate of reducing ripples.

Table 1. Comparative study between the both techniques.

	Conventional indirect FOC strategy	Designed indirect FOC-FOPI-PSO strategy
DR	Slow	Fast
Controller	PI	FOPI-PSO
Block of estimation	Yes	Yes
Modulation technique	PWM	PWM
Power ripple	High	Low
Robustness	Low	High
THD value of current	High	Low
Simplicity	Simple	Simple
Applied to multi-phase generator	Easily	Easily
Implementation	Easy	Easy
Current quality	Low	High
Power quality	Low	High
Completion cost	Not expensive	Not expensive

5.1. Design of the MPPT-FOPI-PSO Technique

The objective of this control structure is to regulate the torque of the DPIG to maintain the mechanical speed at its reference. A FOPI-PSO is used to ensure precise speed control, which allows good tracking of the MPPT.

The structure of the designed MPPT-FOPI-PSO is shown in Figure 8. This designed MPPT is uncomplicated and stronger compared to the MPPT. Also, the designed MPPT technology is a modification of the MPPT technology, whereby a FOPI-PSO is used instead of a PI controller.

5.2. Design of the Indirect FOC-FOPI-PSO Technique

The control structure of the RSC uses two proposed FOPI-PSO controllers to regulate independently the Ps and Qs using the quadrature and the direct rotor current components, respectively. A general RSC control structure is shown in Figure 9. This IFOC-FOPI-PSO is a more simple, robust algorithm, and minimizes more energy ripples compared to the IFOC-PI.

The principle of the designed technique is very simple and depends on the use of the PSO-FOPI in the IFOC-PI in place of the classical PI to improve the efficiency of the IFOC-PI. Also, reducing torque, current, and *Ps* fluctuations. Also, improved DR to *Qs* and *Ps*. The use of the designed IFOC-FOPI-PSO strategy greatly improves the current quality and makes it sinusoidal in shape without ripples, and this is the main objective of this paper.

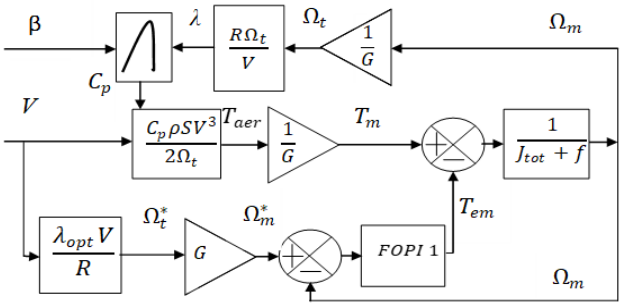

Fig. 8. Block diagram of speed control with FOPI controller.

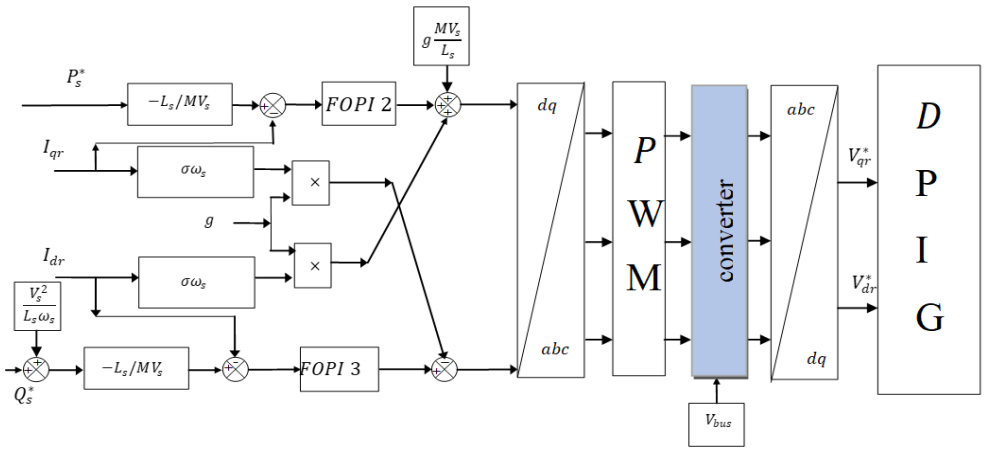

Fig. 9. Proposed technique.

In the designed technique, the control parameters of the PSO technique, used to optimize this problem, are given in Table 2.

Table 2. PSO parameters.

Parameter	Value
w	0.8
c_1	0.1
Swarm size	25
c_2	1.2
Max iteration	50

6. Results

To examine the characteristics of the IFOC-FOPI-PSO, a WTS is developed in MATLAB software and simulated for two proposed tests (tracking and robustness tests).

Table 4 and Table 3 give the numerical values of the parameters of the DPIG, the 1.5 MW WTS, and the GSC respectively. The nine optimal parameters of the three FOPI controllers (FOPI 1, FOPI 2 and FOPI 3), obtained by the PSO technique, are given in Table 5.

Table 3. WTS parameters.

Parameter	Value
Radius of rotor	47 m
Density of air ρ	1.225 Kg/m^3
Gear ratio	90
Number of blade	3

Table 4. DPIG and GSC parameters.

Parameter	Value
Vs	380/690V
Moment of inertia	127 Nm.s^2
Stator resistance	2.6 mΩ
Filter resistance	0.4 mΩ
Ls	2.6 mH
Rr	2.9 mΩ
Lm	2.5 mH
Lr	2.6 mH
DC link voltage	1150 V
Filter inductance	0.4 mH
p	2
DC bus capacitance	0.08 F
Viscous friction coefficient	0.001 Kg.m/s

Table 5. FOPI parameters.

Controller	K_p	K_i	δ
FOPI 1	7.2643e+06	1.8719e+08	0.8925
FOPI 2	30.7512	30.8521	0.0001
FOPI 3	22.9218	35.6307	0.0001

Figure 10 shows that the DPIG speed (Omega) closely follows its reference (Omega*), which means that the MPPT-FOPI-PSO strategy works very well and the DPIG injects into the grid the maximum energy that can be extracted from the kinetic power of the WP.

6.1. Test 1

In this section, the competence of the IFOC-FOPI-PSO is studied in comparison with the traditional technique by tracking references, as well as in terms of the energy ripples.

The WT speeds of the IFOC-FOPI-PSO and IFOC-PI strategies are shown in Figure 11. From this figure, the turbine speed in the case of both controls follows the reference well with preference to the IFOC-FOPI-PSO using the MPPT-FOPI-PSO.

The MPPT-FOPI-PSO reduced static error compared to the MPPT-PI (Figure 12).

Figures 13 and 14 show that the *Qs* and *Ps* follow their references, provided by the MPPT-FOPI-PSO strategy, for the two controllers (PI and PSO-FOPI), and the behaviour is very close in terms of DR. However, better power control precision is obtained with the designed IFOC-FOPI-PSO. Also, the *Ps* is affected by WS, which changes with the change in WS. As for the *Qs*, its value is next to the value 0 VAR with the presence of ripples.

In terms of SSE and RT, the IFOC-FOPI-PSO provided satisfactory results compared to the IFOC-PI, and this is shown by the reduction percentages recorded in Tables 6 and 7. In terms of overshoot of *Qs* and *Ps*, the IFOC-FOPI-PSO provided undesirable values compared to the IFOC-PI. This is shown by the low ratios compared to the IFOC-PI (Table 6).

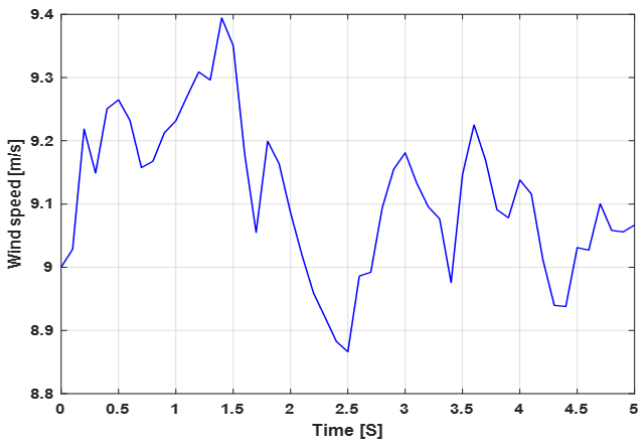

Fig. 10. WS profile.

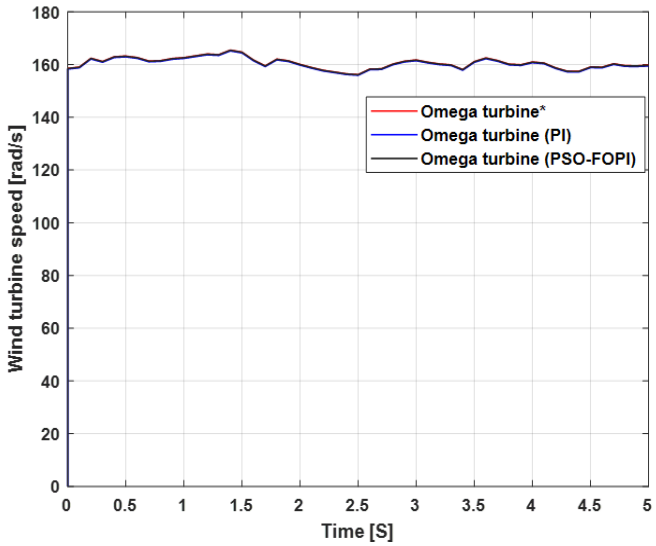

Fig. 11. Wind turbine speed.

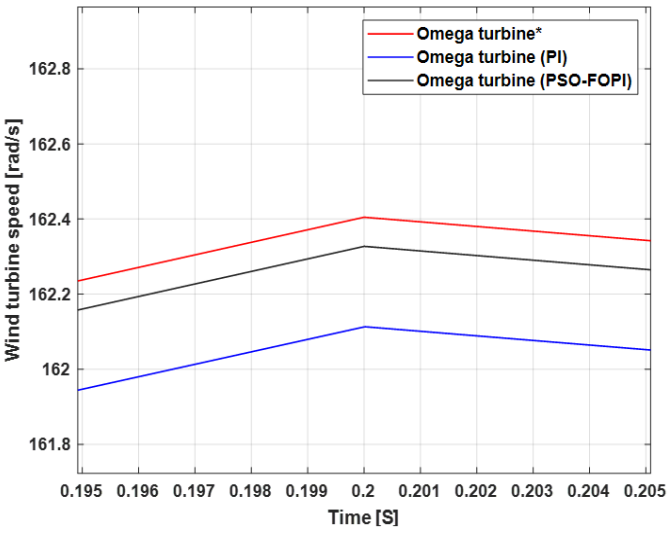

Fig. 12. Zoom in the wind turbine speed.

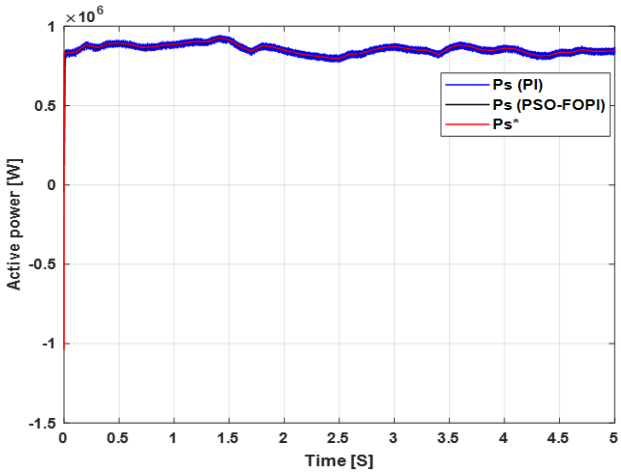

Fig. 13. Active power (first test).

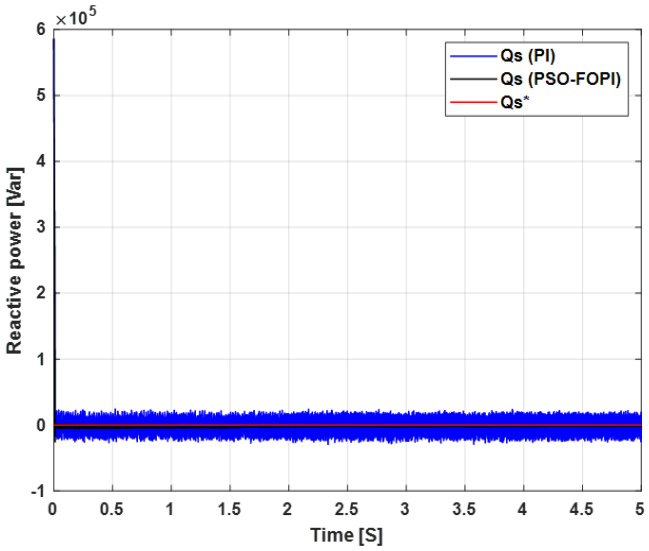

Fig. 14. Reactive power (first test).

Table 6. Numerical values (first test).

		Ps (W)	*Qs* (VAR)
Overshoot	PI	7650	15000
	FOPI-PSO	8980	25000
	Ratios (%)	-17.38	-66.66
SSE	PI	22000	24000
	FOPI-PSO	2400	2200
	Ratios (%)	89.09	90.83
Time response (ms)	PI	0.0119	0.01045
	FOPI-PSO	0.0116	0.01015
	Ratios (%)	2.52	2.87

Figure 15 shows the evolution of the stator currents obtained by both controls. The amplitude of the current follows the evolution of the *Ps* because the amplitude of the grid voltage is assumed to be constant and the shape that the current takes is the sinusoidal shape.

Figure 16 shows the zoom in the current, *Qs*, and *Ps* of both controls, it is clear that there is a minimization of the energy ripples obtained by the IFOC-FOPI-PSO compared to the IFOC-PI. This reduction of power ripples is the result of using the FOPI-PSO which also helped reduce and improve stator power error. Moreover, through the results, the use of the FOPI-PSO leads to an enhancement in the RT for both *Ps* and *Qs* compared to the PI.

Figure 16c shows that the currents have sinusoidal shapes without ripples in the case of the IFOC-FOPI-PSO, which implies clean power without harmonics injected into the grid.

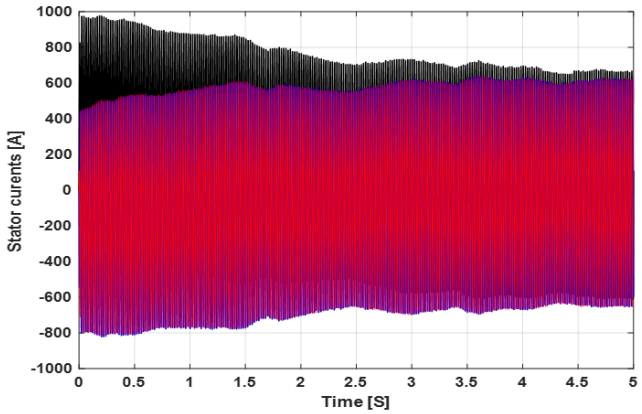

a) Indirect FOC-FOPI-PSO strategy.

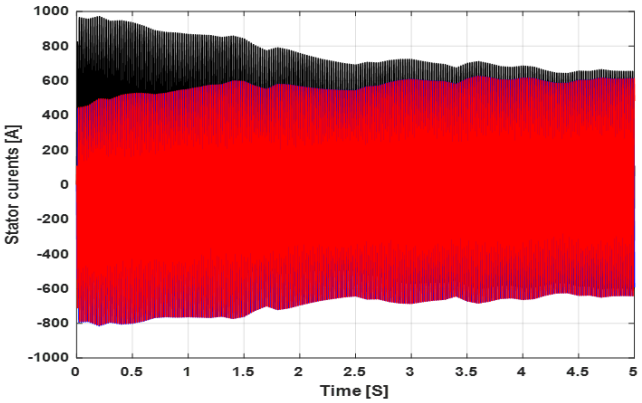

b) Indirect FOC strategy.

Fig. 15. Stator current (test 1).

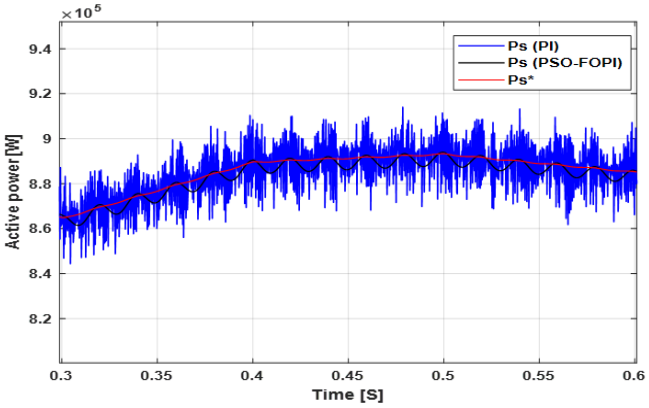

a) *Ps*.

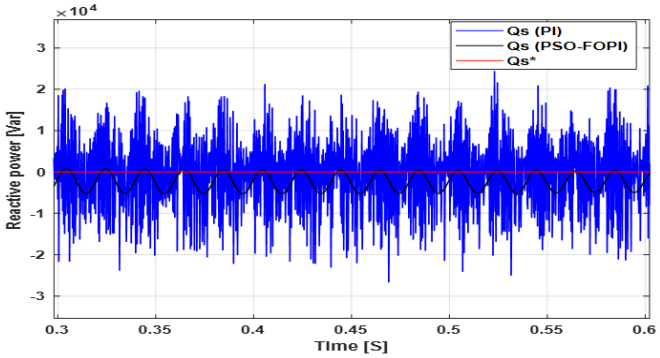

b) *Qs*.

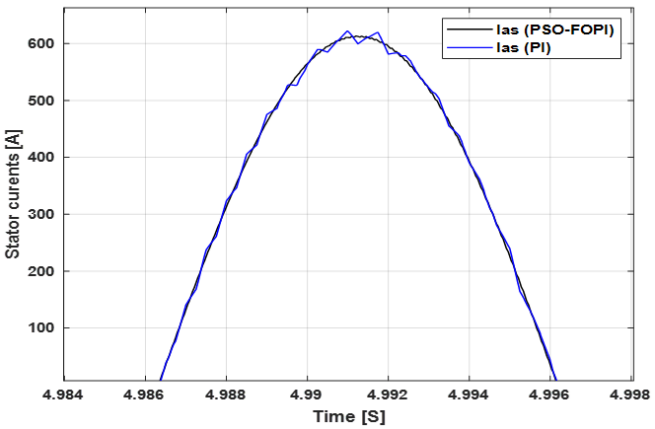

c) Stator current.

Fig. 16. Zoom in the current, *Ps*, and *Qs* (test 1).

The current THD is represented in Figures 17a and 17b for both control schemes. Through these two forms, the designed indirect FOC-FOPI-PSO strategy gave a lower THD than the indirect FOC technique, and the ratio of THD minimization was about 99.46%**.** Through this value, it can be said that the designed control is more efficient in improving the current quality and energy than classical control, and it is the top solution for regulating machines.

Figure 18 clearly shows that the DC bus voltage follows its reference very well. In the DC voltage control loop, a classical PI is used since it provides good performance under various WSs.

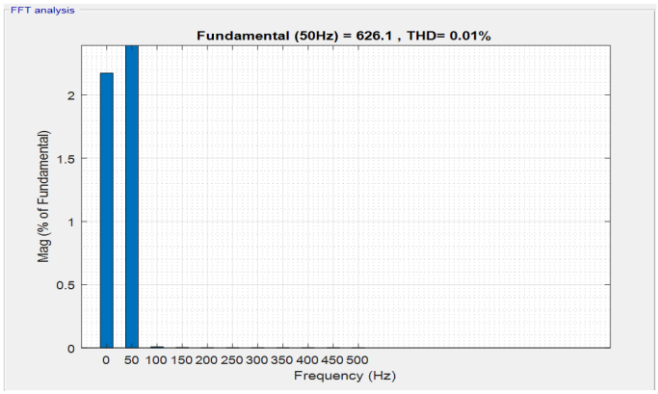

a) Indirect FOC-FOPI-PSO.

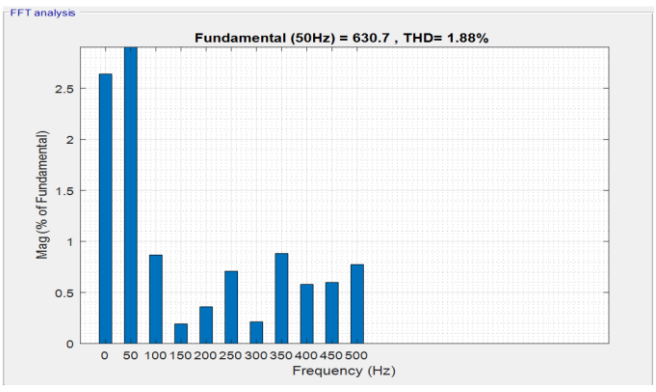

b) Indirect FOC strategy.

Fig. 17. Current THD (first test).

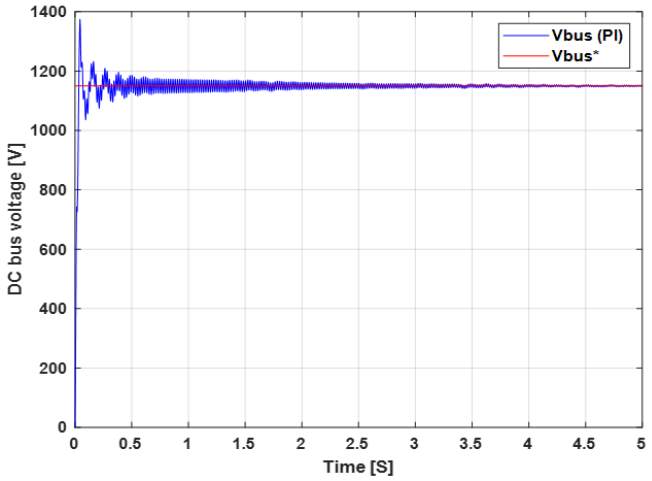

Fig. 18. The DC bus voltage (test 1).

In Table 7, the ripple minimization ratios for the current, *Ps*, and *Qs* are presented for both the proposed and IFOC-PI. Through this value, it can be said that the FOC-FOPI-PSO is more effective in meliorating the current and power quality than the classical method, and this is shown by the high minimization ratios, where the ratios were 90.90%, 80.24%, and 89.44% for each of the *Qs*, *Ps*, and current, respectively.

Table 7. Comparison of ripple values between strategies.

	Qs (VAR)	*Ps* (W)	*Ias* (A)
IFOC	30570	33000	18
IFOC-FOPI-PSO	6040.70	3000	1.9
Ratios	80.24%	90.90%	89.44%

6.2. Second Test

In this section, the behaviour of the IFOC-FOPI-PSO is studied in comparison with the conventional indirect FOC in the case of changing L_r, L_s, R_s, R_r, and L_m to the following new values 0.0052 H, 0.0052 H, 0.0052 Ω, 0.0050 H, and 0.0058 Ω, respectively. The results are shown in Figures 19 to 23.

Through figures 19 and 20, the *Ps* and *Qs* follow well the references, with always preference for the IFOC-FOPI-PSO in terms of undulation minimization and DR. The IFOC-FOPI-PSO provided excellent results in terms of RT and SSE compared to the IFOC-PI. From Table 8, the IFOC-FOPI-PSO minimized the RT and SSE of DPIG power by significant percentages. However, the disadvantage of the IFOC-FOPI-PSO is represented in the high values of overshoot, as it provided unsatisfactory results in terms of overshoot values compared to the PI-IFOC. Also, the IFOC-PI has reduced the overshoot of *Qs* and *Ps* in significant proportions compared to the IFOC-PI.

The electric current is shown in Figure 21, where it is noted that the current remains in the form of *Ps*. From Figure 22, the IFOC-FOPI-PSO reduced the current ripples compared to the PI-IFOC.

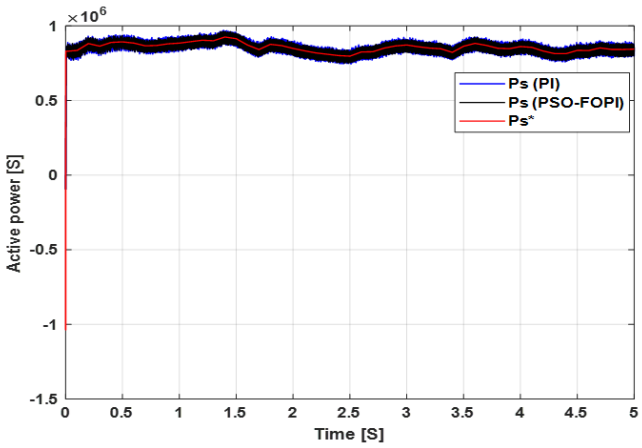

Fig. 19. *Ps* (test 2).

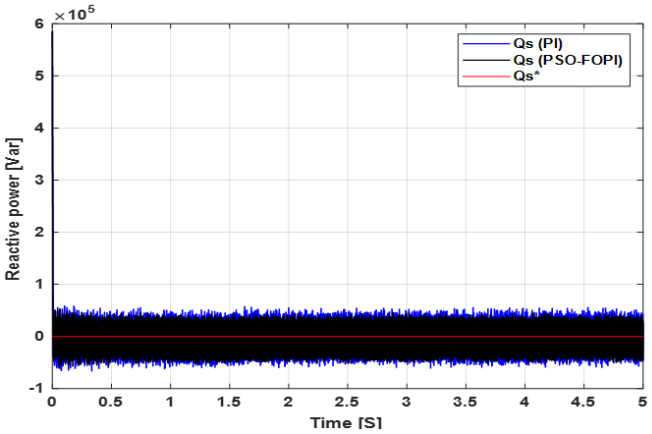

Fig. 20. *Qs* (test 2).

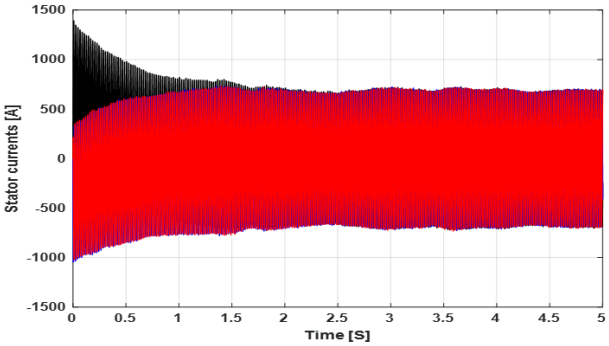

(a) IFOC-FOPI-PSO strategy.

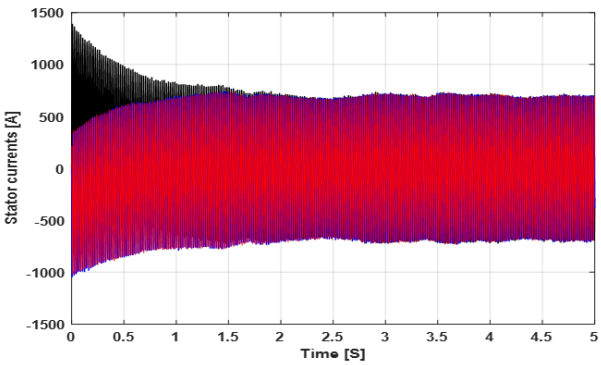

(b) IFOC-PI strategy.

Fig. 21. Stator current (second test).

Table 8. Numerical values (test 2).

		Ps (W)	*Qs* (VAR)
Overshoot	PI	16800	13500
	FOPI-PSO	28000	22570
	Ratios (%)	-66.66	67.18
SSE	PI	41200	48880
	FOPI-PSO	8800	18070
	Ratios (%)	76.64	63.03
Time response (ms)	PI	0.0054	0.0054
	FOPI-PSO	0.0053	0.0049
	Ratios (%)	1.85	9.25

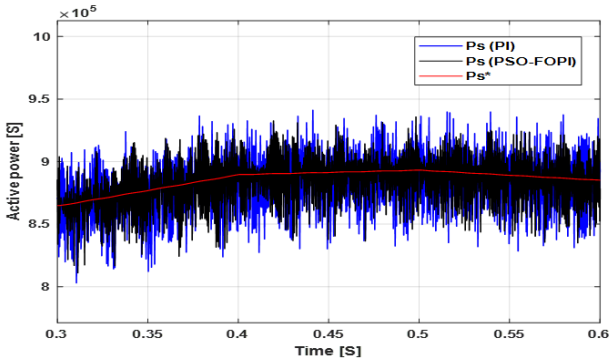

(a) *Ps*.

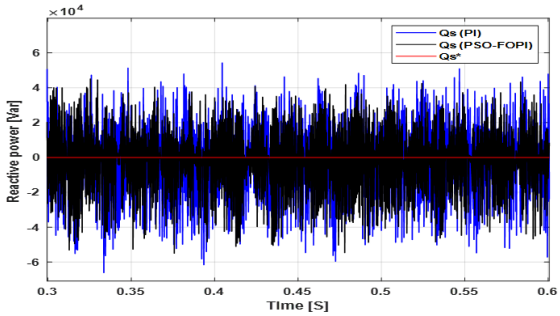

(b) *Qs*.

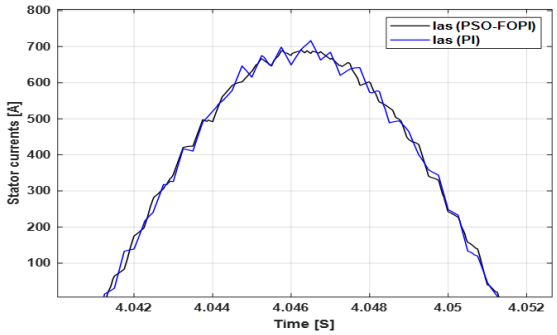

(c) *Ias*.

Fig. 22. Zoom in the *Ias*, *Ps*, and *Qs* (Second test).

The IFOC-FOPI-PSO significantly minimized the ripples of the *Qs*, current, and *Ps* compared to the PI-IFOC and this is shown in Figure 22. The current THD was 2.61% and 3.50% for the IFOC-FOPI-PSO and the PI-IFOC, respectively (see Figure 23). So, the IFOC-FOPI-PSO reduced the current THD by 25.42% compared to the PI-IFOC. This ratio indicates the characteristic of the IFOC-FOPI-PSO in improving the EP quality despite a change in the DPIG parameters.

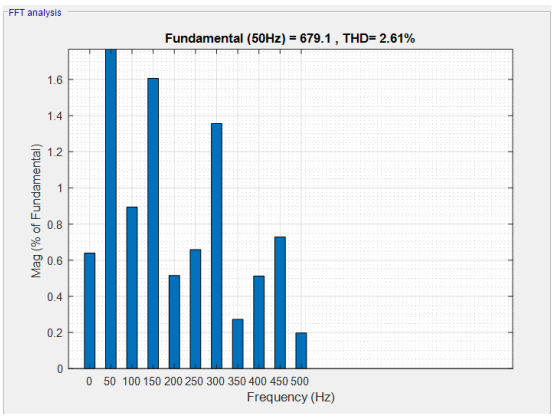

(a) IFOC-FOPI-PSO.

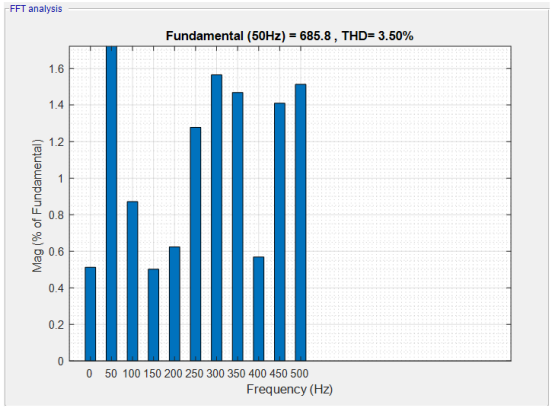

(b) IFOC-PI.

Fig. 23. Current THD (test 2).

Figure 24 represents the DC bus voltage, where this voltage follows the reference well with large ripples due to changing the generator parameters. Also, this voltage is a constant value and equal to 1150 V. Moreover, an overrun of the threshold value is observed at the beginning. This overshoot takes a significant value, as this value is large and affects the inverter greatly, which is undesirable.

In Table 9, the values of ripples are presented for the *Qs*, current, and *Ps* of the IFOC-FOPI-PSO and IFOC-PI together. Also, reduction ratios for these ripples are given. Through the reduction ratios, it can be said that the IFOC-FOPI-PSO is more effective in this test in terms of reducing energy and current ripples compared to the IFOC-PI. The designed IFOC-FOPI-PSO reduced the ripples by ratios estimated at 31.57%, 70%, and 96.66% for each of the *Ps*, current, and *Qs*, respectively.

The suggested control scheme in terms of THD is the best compared to some of the suggested controls published in several articles such as DTC, DPC, and backstepping control. A comparative study between the IFOC-FOPI-PSO and the published works is shown in Table 10. Therefore, it can be said that the IFOC-FOPI-PSO is one of the best controls that can be designed and used in the control of machines. On the other hand, the designed technique is compared with published works in terms of the ratios of ripple minimization and the RT of the *Ps* and *Qs*, to know the extent of its effectiveness compared to other strategies.

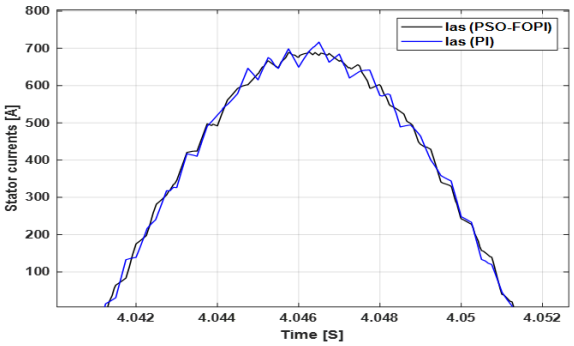

Fig. 24. The DC bus voltage (test 2).

Table 9. Comparison of ripple values between both controls.

	Qs (VAR)	*Ps* (W)	*Ias* (A)
IFOC-PI	596000	57000	40
IFOC-FOPI-PSO	19880	39000	12
Ratios	96.66%	31.57%	70%

Table 10. Comparison between the proposed control and other articles in terms of the THD.

Reference	Methods		THD (%)
[73]	FOC		3.7
[76]	GA-least squares wavelet support vector machines		3.39
[77]	Power control	First technique	5.6817
		Second technique	3.1873
[78]	Integral SMC		9.71
	Multi-resonant-based SMC		3.14
[25]	DTC		6.70
	Fuzzy DTC strategy		2.40
[79]	DPC-STA		1.66
[80]	DTC		7.83
	Neural DTC		3.26
[81]	L-filter-based DTC		10.79
	LCL-filter-based DPC		4.05
[82]	Virtual flux DPC strategy		4.88
	DPC		4.19
[83]	Second-order SMC		3.13
[84]	2-level DTC		8.75
	3-level DTC		1.57
[85]	Integral SMC		0.88
[13]	First-order SMC		2.56
	High-order SMC		1.08
Designed strategy	IFOC-FOPI-PSO strategy		0.01

The comparison results are listed in Table 11 that shows that the designed strategy has very high ripple minimization rates compared to several published articles. Moreover, the IFOC-FOPI-PSO offers a much better *Ps* and *Qs* RT compared to most strategies published in scientific works. So, the IFOC-FOPI-PSO can be proposed as a solution to control machines because of the results obtained and the ease of realization compared to several controls.

The superior performance of the proposed FOPI-PSO controller can be attributed to several technical factors. First, the inclusion of the fractional-order term δ introduces an additional degree of freedom that enhances the frequency-domain shaping of the regulator. This allows for more precise attenuation of low-frequency disturbances and improved damping of energy oscillations—capabilities that conventional PI or first-order hybrid regulators lack.

Second, the PSO tuning mechanism performs a global search over both gain parameters and the fractional order, avoiding local minima and enabling optimal trade-offs between fast response, low overshoot, and minimal SSE.

Third, the swarm configuration—including population size, inertia weight, and acceleration coefficients—was selected to balance exploration and exploitation, leading to stable convergence and highly effective parameter adaptation.

Collectively, these design features explain why the designed IFOC–FOPI-PSO method consistently outperforms previously reported techniques in minimizing current THD, minimizing *Ps* ripple, and enhancing robustness under parameter variations.

By clarifying the selection criteria and linking the observed improvements to specific regulator characteristics, the comparative analysis becomes more scientifically grounded and demonstrates with greater rigor why the designed technique achieves superior results.

Table 11. A comparative study between the IFOC-FOPI-PSO and other articles in terms of the power ripple ratios and time response

		Energy ripples ratios (%)		Time response (ms)	
		Ps	*Qs*	*Ps*	*Qs*
[11]		41.17	94	-	-
[36]		-	-	33.8	34.5
[85]		-	75.2	-	280
[86]		13.44	8.96	-	-
[87]	DPC	-	-	17	18
	Nonlinear DPC			9	5
[26]	NN-DPC	66.29	45.26	-	-
	NN-FL-DPC	67.13	57.74		
Proposed strategy		90.90	80.24	0.0116	0.01015

7. Practical Feasibility and Implementation Considerations

Although the results presented in this work are based on detailed simulations, the proposed IFOC–FOPI-PSO controller is suitable for real-time implementation, and several practical considerations support its feasibility.

First, the computational burden of the controller during online operation is comparable to that of a standard PI regulator. Once the PSO algorithm determines the optimal gains and fractional order, the controller operates using simple algebraic and fractional-integration terms that can be efficiently executed on modern DSPs or FPGAs. Recent advancements in embedded digital fractional-order operators further reduce the overhead associated with implementing non-integer calculus in real time.

Second, the PSO optimization is performed offline, meaning convergence time does not affect real-time control performance. Typical swarm sizes and iteration counts used in this study reach convergence within seconds to minutes on standard desktop hardware, making the tuning procedure practical during the system-design phase or scheduled maintenance periods.

Third, the proposed method requires no supplementary control loops, observers, or PLL-based synchronization blocks, which simplifies hardware deployment compared to more complex hybrid or intelligent controllers reported in the literature. This contributes to lower implementation complexity and reduces sensitivity to measurement noise or digital delays.

To further enhance confidence in real-world applicability, future work will include hardware-in-the-loop (HIL) testing using a real-time simulator and an embedded controller. This will allow validation of the controller's behavior under converter switching, sensor noise, communication delays, and DPIG parameter drift—factors not fully captured in simulation. Ultimately, this step will provide a necessary bridge between simulation and full-scale experimental deployment on a laboratory test bench or prototype wind-turbine setup.

Although the proposed IFOC–FOPI-PSO regulator demonstrates strong performance under balanced and parameter-varying operating conditions, its robustness against unbalanced grid voltage faults has not yet been evaluated. Such conditions—commonly occurring during single-phase faults, voltage dips, or distribution asymmetries—can introduce negative-sequence components, torque pulsations, increased current distortion, and instability in DPIG-based wind systems. Including a dedicated test under unbalanced grid scenarios would provide deeper insight into the regulator's ability to maintain power quality and dynamic stability when subjected to asymmetrical disturbances. This assessment would also clarify how well the fractional-order dynamics and PSO-tuned parameters suppress negative-sequence effects compared to traditional PI-based FOC.

Incorporating these tests, either through simulation or future hardware-in-the-loop experiments, would significantly strengthen the validation and demonstrate the full robustness of the designed control technique under realistic grid-fault conditions.

8. Conclusions

This work introduced a novel control strategy for DPIG-based wind-turbine systems using a fractional-order PI controller optimized via Particle Swarm Optimization (FOPI-PSO). The modelling of the DPIG-driven wind turbine and the MPPT scheme was first presented, providing the active-power reference for the control loops. The proposed intelligent controller was then integrated into the field-oriented control (FOC) framework to regulate both active (*Ps*) and reactive (*Qs*) power, combining the flexibility of fractional-order dynamics with the global optimization capability of PSO.

A detailed analysis of the IFOC–FOPI-PSO scheme highlighted its main advantages—namely improved dynamic shaping, robustness to parameter variations, and compatibility with the standard FOC structure—while maintaining the simplicity of classical PI implementation. Unlike previous hybrid or fractional-order controllers reported in [37], [38], and [44], which often increase computational burden or modify the control architecture, the proposed method achieves performance gains without additional structural complexity.

Simulation results demonstrate substantial improvements: a 99.46% reduction in current THD, a 90.90% decrease in active-power oscillations, and an 89.09% reduction in steady-state error, along with a measurable enhancement in transient response. These outcomes confirm the effectiveness and novelty of the FOPI-PSO controller as a high-performance and computationally efficient solution for DPIG-based wind-energy conversion systems. The findings also show that the proposed controller maintains strong robustness under generator-parameter variations, achieving significantly lower *Ps* and *Qs* ripple across different operating conditions. Current waveforms remain of high quality with very low THD, and the method operates reliably without requiring a phase-locked loop. However, the IFOC–FOPI-PSO exhibits slightly less favourable overshoot characteristics compared with conventional IFOC–PI control. Furthermore, the present validation is limited to simulation results.

Future work will focus on hardware implementation and experimental testing to verify the practical performance of the proposed controller and to confirm the improvements observed in the simulation study.

Nomenclature

RE	Renewable energies
DPIG	Double powered induction generator
WP	Wind power
PI	Proportional-integral controller
PID	Proportional-integral derivative controller
IG	İnduction generator
PWM	Pulse width modulation
WTS	Wind turbine system

RSC	Rotor side converter
WT	Wind turbine
SVM	Space vector modulation
GA	Genetic Algorithm
STC	Super-twisting control
THD	Total harmonic distortion
GA	Genetic algorithm
FOC	Field-oriented control
IFOC	İndirect field-oriented control
BC	Backstepping control
FL	Fuzzy logic
GSC	Grid side converter
SMC	Sliding mode control
MPPT	Maximum power point tracking
ST	Switching table
WPCS	Wind power conversion system
EP	Electrical power

Author Contributions

Conceptualization, H.B., H.G., and N.B.; methodology, H.B., H.G., and N.B.; software, H.B., H.G., and N.B.; validation, H.B. and H.G.; formal analysis, H.B., H.G., N.B., and T.T.; investigation, H.G., H.B., and T.T.; resources, H.G. and H.B.; data curation, H.B., H.G., N.B., and T.T.; writing-original draft preparation, H.B., H.G., and N.B.; writing-review and editing, H.B., H.G., N.B., and T.T.; visualization, H.B., H.G., N.B., and T.T.; supervision, H.B., H.G., N.B., and T.T.; project administration, H.G. and H.B.; funding acquisition, N.B. and H.B. All authors have read and agreed to the published version of the manuscript.

Acknowledgements

Not applicable.

Conflict of Interest

The authors declare no conflict of interest.

References

[1] G. Abad, J. Lopez, M. A. Rodriguez, L. Marroyo, and G. Iwanski, *Doubly Fed Induction Machine: Modeling and Control for Wind Energy Generation*. New Jersey, United States: Wiley-IEEE Press, 2011.

[2] C. Bhattacharjee, A. K. Roy, and B. K. Roy, "Improvement of available load voltage for a constant speed WECS coupled with fuzzy-controlled DSTATCOM," in *Proc. IEEE 15th Int. Conf. Harmonics and Quality of Power*, 2012, pp. 637–641.

[3] K. Qin, S. Wang, and Z. Kang, "Research on zero-voltage ride through control strategy of doubly fed wind turbine," *Energies*, vol. 14, no. 8, p. 2287, 2021.

[4] L. Vyshnevskyi, M. Mukha, and D. Vyshnevskyi, "Discrete-pulse voltage control of an asynchronous generator," in *Proc. IEEE Int. Conf. Modern Electrical and Energy Systems*, 2021, pp. 1–4.

[5] E. Hossein and F. Jawad, "Operation principles, structure, and design of synchronous generators," in *Electromagnetic Analysis and Condition Monitoring of Synchronous Generators*. IEEE, 2023, pp. 9–54.

[6] Y. Liu, J. Ou, and M. Noe, "A large-scale superconducting DC wind generator considering concentrated/distributed armature winding," *IEEE Trans. Appl. Supercond.*, vol. 27, no. 4, pp. 1–5, 2017.

[7] D. M'Hamed, A. Abdel Ghani, A. Mohamed, T. Ahmed, and T. Khalfallah, "Robust fuzzy gains scheduling of RST controller for a WECS based on a doubly-fed induction generator," *Automatika*, vol. 57, no. 3, pp. 617–626, 2016.

[8] P. Kroplewski, M. Morawiec, A. Jąderko, and C. Odeh, "Simulation studies of control systems for doubly fed induction generator supplied by the current source converter," *Energies*, vol. 14, no. 5, p. 1511, 2021.

[9] J. M. Bundi, X. Ban, D. W. Wekesa, and X. Huang, "Linear robust control methods for a doubly fed induction generator at steady states," in *Proc. IEEE IECON – Industrial Electronics Society Annual Conference*, 2020, pp. 3230–3235.

[10] K. Ouezgan, B. Bossoufi, and M. N. Bargach, "DTC control of DFIG-generators for wind turbines: FPGA implementation based," in *Proc. Int. Renewable and Sustainable Energy Conf.*, 2017, pp. 1–6.

[11] B. Habib, M. Fayçal, and S. Lemdani, "New direct power synergetic-SMC technique based PWM for DFIG integrated to a variable speed dual-rotor wind power," *Automatika*, vol. 63, no. 4, pp. 718–731, 2022.

[12] I. Yaichi, A. Harrouz, I. Boussaid, A. Semmah, P. Wira, I. Colak, and K. Kayisli, "An improved DTC strategy for a DFIG using an artificial neural network controller," in *Proc. Int. Conf. Smart Grid*, 2021, pp. 231–237.

[13] E. K. Djamel, M. Abdelkader, B. Larbi, and A. P. M. V. Den Bossche, "A comprehensive review of LVRT capability and sliding mode control of grid-connected wind-turbine-driven doubly fed induction generator," *Automatika*, vol. 57, no. 4, pp. 922–935, 2016.

[14] H. Benbouhenni and N. Bizon, "Terminal synergetic control for direct active and reactive powers in asynchronous generator-based dual-rotor wind power systems," *Electronics*, vol. 10, no. 16, p. 1880, 2021.

[15] M. Abdelrahem, C. Hackl, R. Kennel, and J. Rodriguez, "Low sensitivity predictive control for doubly-fed induction generators based wind turbine applications," *Sustainability*, vol. 13, no. 16, p. 9150, 2021.

[16] P. Xiong and D. Sun, "Backstepping-based DPC strategy of a wind turbine-driven DFIG under normal and

harmonic grid voltage," *IEEE Trans. Power Electron.*, vol. 31, no. 6, pp. 4216–4225, 2016.

[17] Y. Han and R. Ma, "Adaptive-gain second-order sliding mode direct power control for wind-turbine-driven DFIG under balanced and unbalanced grid voltage," *Energies*, vol. 12, no. 20, p. 3886, 2019.

[18] Y. Han, S. Li, and C. Du, "Adaptive higher-order sliding mode control of series-compensated DFIG-based wind farm for sub-synchronous control interaction mitigation," *Energies*, vol. 13, no. 20, p. 5421, 2020.

[19] H. Benbouhenni, "Intelligent super twisting high order sliding mode controller of dual-rotor wind power systems with direct attack based on doubly-fed induction generators," *J. Electr. Eng., Electron., Control Comput. Sci.*, vol. 7, no. 4, pp. 1–8, 2021.

[20] M. Samir, M. Said, N. Ali, S. Youcef, and O. M'Hamed, "An optimized fractional order PI controller to improve DFIG active and reactive powers control," in *Proc. Int. Symp. Advanced Topics in Electrical Engineering*, 2021, pp. 1–6.

[21] X.-Z. Lv, Z.-J. Kang, and Y.-C. Mei, "Double dq control strategy of DFIG based on passivity theory under unbalanced grid voltage," in *Proc. Chinese Control Conf.*, 2013, pp. 8851–8856.

[22] H. Benbouhenni, Z. Boudjema, and A. Belaidi, "Power control of DFIG in WECS using DPC and NDPC-NPWM methods," *Math. Model. Eng. Probl.*, vol. 7, no. 2, pp. 223–236, 2020.

[23] Y. Sahri, S. Tamalouzt, B. S. Lalouni, S. Bacha, N. Ullah, A. A. A. Ahamdi, and A. N. Alzaed, "Advanced fuzzy 12 DTC control of doubly fed induction generator for optimal power extraction in wind turbine system under random wind conditions," *Sustainability*, vol. 13, no. 21, p. 11593, 2021.

[24] R. D. Moulay, E. Ahmed, and C. Mohamed, "Neural networks for stable control of nonlinear DFIG in wind power systems," *Procedia Comput. Sci.*, vol. 127, pp. 454–463, 2018.

[25] W. Ayrira, M. Ourahoua, B. El Hassounia, and A. Haddib, "Direct torque control improvement of a variable speed DFIG based on a fuzzy inference system," *Math. Comput. Simul.*, vol. 167, pp. 308–324, 2020.

[26] S. Younes, T. Salah, H. Farid, S. L. B., B. Mohit, M. M. A., M. S. A., and S. S. M. Ghoneim, "New intelligent direct power control of DFIG-based wind conversion system by using machine learning under variations of all operating and compensation modes," *Energy Rep.*, vol. 7, pp. 6394–6412, 2021.

[27] B. Habib, "Application of DPC and DPC-GA to the dual-rotor wind turbine system with DFIG," *Int. J. Robot. Autom.*, vol. 10, no. 3, pp. 224–234, 2021.

[28] E. Heydari, M. Rafiee, and M. Pichan, "Fuzzy-genetic algorithm-based direct power control strategy for DFIG," *Iran. J. Electr. Electron. Eng.*, vol. 14, no. 4, pp. 353–361, 2018.

[29] S. Labdai, B. Hemici, L. Nezli, N. Bounar, A. Boulkroune, and L. Chrifi-Alaoui, "Control of a DFIG-based WECS with optimized PI controllers via a duplicate PSO algorithm," in *Proc. Int. Conf. Control, Automation and Diagnosis*, 2019, pp. 1–6.

[30] A. Khurshid, M. A. Mughal, A. Othman, T. Al-Hadhrami, H. Kumar, I. Khurshid, and J. A. Arshad Ahmad, "Optimal pitch angle controller for DFIG-based wind turbine system using computational optimization techniques," *Electronics*, vol. 11, no. 8, p. 1290, 2022.

[31] S. Zhou, F. Rong, and X. Ning, "Optimization control strategy for large doubly-fed induction generator wind farm based on grouped wind turbine," *Energies*, vol. 14, no. 16, p. 4848, 2021.

[32] A. M. Eltamaly, M. Al-Saud, K. Sayed, and A. G. Abo-Khalil, "Sensorless active and reactive control for DFIG wind turbines using opposition-based learning technique," *Sustainability*, vol. 12, no. 9, p. 3583, 2020.

[33] Y. Li, B. Xiong, Y. Su, J. Tang, and Z. Leng, "Particle swarm optimization-based power and temperature control scheme for grid-connected DFIG-based dish-Stirling solar-thermal system," *Energies*, vol. 12, no. 7, p. 1300, 2019.

[34] B. Habib and S. Lemdani, "Combining synergetic control and super twisting algorithm to reduce the active power undulations of doubly fed induction generator for dual-rotor wind turbine system," *Electr. Eng. Electromech.*, no. 3, pp. 8–17, 2021.

[35] B. Habib and N. Bizon, "A synergetic sliding mode controller applied to direct field-oriented control of induction generator-based variable speed dual-rotor wind turbines," *Energies*, vol. 14, no. 15, pp. 1–17, 2021.

[36] F. Echiheb, Y. Ihedrane, B. Bossoufi, M. Bouderbala, S. Motahhir, M. Masud, S. Aljahdali, and M. ElGhamrasni, "Robust sliding-backstepping mode control of a wind system based on the DFIG generator," *Sci. Rep.*, vol. 12, p. 11782, 2022.

[37] J.-Y. Cao and B.-G. Cao, "Design of fractional order controllers based on particle swarm optimization," in *Proc. IEEE Conf. Industrial Electronics and Applications*, 2006, pp. 1–6.

[38] X. Liu, "Optimization design on fractional order PID controller based on adaptive particle swarm optimization algorithm," *Nonlinear Dyn.*, vol. 84, pp. 379–386, 2016.

[39] M. Zamani, M. K. Ghartemani, N. Sadati, and M. Parmiani, "Design of a fractional order PID controller for an AVR using particle swarm optimization," *Control Eng. Pract.*, vol. 17, no. 12, pp. 1381–1387, 2009.

[40] B. Habib, Z. Boudjema, and A. Belaidi, "Higher control scheme using neural second order sliding mode and ANFIS-SVM strategy for a DFIG-based wind turbine,"

Int. J. Adv. Telecommun., Electrotech., Signals Syst., vol. 8, no. 2, pp. 17–28, 2019.

[41] B. Habib, "Hybrid neural sliding mode control of a DFIG speed in wind turbines," *Majlesi J. Energy Manag.*, vol. 6, no. 4, pp. 31–41, 2017.

[42] F. Mazouz, S. Belkacem, S. Drid, L. Chrifi-Alaoui, and I. Colak, "Fuzzy sliding mode control of DFIG applied to the WECS," in *Proc. Int. Conf. Systems and Control*, 2019, pp. 465–470.

[43] H. Benbouhenni, "ANFIS-sliding mode control of a DFIG supplied by a two-level SVPWM technique for wind energy conversion system," *Int. J. Appl. Power Eng.*, vol. 9, no. 1, pp. 36–47, 2020.

[44] M. T. Hagh, S. Roozbehani, F. Najaty, S. Ghaemi, Y. Tan, and K. M. Muttaqi, "Direct power control of DFIG-based wind turbine based on wind speed estimation and particle swarm optimization," in *Proc. Australasian Universities Power Engineering Conf.*, 2015, pp. 1–6.

[45] M. E. Zarei and B. Asaei, "Combined vector control and direct power control methods for DFIG under normal, unbalanced and distorted grid voltage conditions," in *Proc. Int. Power Electronics, Drive Systems and Technologies Conf.*, 2013, pp. 107–112.

[46] P. Q. Dzung, N. B. Anh, and H. L. Hong, "New artificial neural network based direct virtual torque control and direct power control for DFIG in wind energy systems," in *Proc. IEEE Int. Conf. Power Electronics and Drive Systems*, 2011, pp. 219–227.

[47] L. Shang and J. Hu, "Sliding-mode-based direct power control of grid-connected wind-turbine-driven doubly fed induction generators under unbalanced grid voltage conditions," *IEEE Trans. Energy Convers.*, vol. 27, no. 2, pp. 362–373, 2012.

[48] Y. Han, R. Ma, W. Pan, and C. Wang, "A novel super-twisting algorithm-based direct power control strategy for doubly fed induction generator," in *Proc. Asian Control Conf.*, 2019, pp. 1619–1624.

[49] M. Farida, S. Belkacem, and I. Colak, "Fuzzy high order sliding mode control based DPC of DFIG using SVM," in *Proc. Int. Conf. Smart Grid*, 2021, pp. 278–282.

[50] B. Habib and N. Bizon, "Third-order sliding mode applied to the direct field-oriented control of the asynchronous generator for variable-speed contra-rotating wind turbine generation systems," *Energies*, vol. 14, no. 18, pp. 1–17, 2021.

[51] B. Habib and N. Bizon, "Improved rotor flux and torque control based on the third-order sliding mode scheme applied to the asynchronous generator for the single-rotor wind turbine," *Mathematics*, vol. 9, no. 18, p. 2297, 2021.

[52] H. E. Alami, B. Bossoufi, S. Motahhir, E. H. Alkhammash, M. Masud, M. Karim, M. Taoussi, M. Bouderbala, M. Lamnadi, and M. El Mahfoud, "FPGA in the loop implementation for observer sliding mode control of DFIG-generators for wind turbines," *Electronics*, vol. 11, no. 1, p. 116, 2022.

[53] L. Pan, Z. Zhu, Y. Xiong, and J. Shao, "Integral sliding mode control for maximum power point tracking in DFIG-based floating offshore wind turbine and power to gas," *Processes*, vol. 9, no. 6, p. 1016, 2021.

[54] R. Ma, Y. Han, and W. Pan, "Variable-gain super-twisting sliding mode damping control of series-compensated DFIG-based wind power system for SSCI mitigation," *Energies*, vol. 14, no. 2, p. 382, 2021.

[55] H. Benbouhenni, Z. Boudjema, and A. Belaidi, "DFIG-based WT system using FPWM inverter," *Int. J. Smart Grid*, vol. 2, no. 3, pp. 142–154, 2018.

[56] M. Alhato, S. Bouallègue, and H. Rezk, "Modeling and performance improvement of direct power control of doubly-fed induction generator based wind turbine through second-order sliding mode control approach," *Mathematics*, vol. 8, no. 11, p. 2012, 2020.

[57] N. Klaes, F. Pöschke, and H. Schulte, "Grid forming stator flux control of doubly-fed induction generator," *Energies*, vol. 14, no. 20, p. 6766, 2021.

[58] O. G. Oussama and A. Douik, "Comparison between PI and fuzzy controllers in speed control of PMSM," in *Proc. Int. Conf. Green Energy Conversion Systems*, 2017, pp. 1–7.

[59] Y. Naung, A. S. Anatolii, and Y. H. Lin, "Speed control of DC motor by using neural network parameter tuner for PI-controller," in *Proc. IEEE Conf. Russian Young Researchers in Electrical and Electronic Engineering*, 2019, pp. 2152–2156.

[60] P. Pingping, L. Ziguang, L. Zhuo, and W. Di, "PI-PSO algorithm based voltage controller of STATCOM for self-excited induction generator," in *Proc. Chinese Control Conf.*, 2015, pp. 4349–4354.

[61] M. Farhat, M. Hussein, and A. M. Atallah, "Enhancement performance of a three-phase grid connected photovoltaic system based on PI-genetic algorithm controller," in *Proc. Int. Middle East Power Systems Conf.*, 2017, pp. 145–151.

[62] J. Talebi and S. Ganjefar, "Fractional order sliding mode controller design for large scale variable speed wind turbine for power optimization," *Environ. Prog. Sustain. Energy*, vol. 37, no. 6, pp. 2124–2131, 2018.

[63] X. Rui, W. Yin, Y. Dong, L. Lin, and X. Wu, "Fractional-order sliding mode control for hybrid drive wind power generation system with disturbances in the grid," *Wind Energy*, vol. 22, no. 1, pp. 49–64, 2019.

[64] S. Huang, L. Xiong, J. Wang, P. Li, Z. Wang, and M. Ma, "Fixed-time fractional-order sliding mode controller for multimachine power systems," *IEEE Trans. Power Syst.*, vol. 36, no. 4, pp. 2866–2876, 2021.

[65] H. Xue, Y. Bai, H. Hu, T. Xu, and H. Liang, "A novel hybrid model based on TVIW-PSO-GSA algorithm and

support vector machine for classification problems," *IEEE Access*, vol. 7, pp. 27789–27801, 2019.

[66] Z. Han, Y. Li, and J. Liang, "Numerical improvement for the mechanical performance of bikes based on an intelligent PSO-ABC algorithm and WSN technology," *IEEE Access*, vol. 6, pp. 32890–32898, 2018.

[67] N. Geng, Q. Meng, D. Gong, and P. W. H. Chung, "How good are distributed allocation algorithms for solving urban search and rescue problems? A comparative study with centralized algorithms," *IEEE Trans. Autom. Sci. Eng.*, vol. 16, no. 1, pp. 478–485, 2019.

[68] S. Yousaf, A. Mughees, M. G. Khan, A. A. Amin, and M. Adnan, "A comparative analysis of various controller techniques for optimal control of smart nano-grid using GA and PSO algorithms," *IEEE Access*, vol. 8, pp. 205696–205711, 2020.

[69] H. Abbasi, M. Ghanbari, R. Ebrahimi, and M. Jannati, "IRFOC of induction motor drives under open-phase fault using balanced and unbalanced transformation matrices," *IEEE Trans. Ind. Electron.*, vol. 68, no. 10, pp. 9160–9173, 2021.

[70] T.-D. Ton, M.-F. Hsieh, and P.-H. Chen, "A novel robust sensorless technique for field-oriented control drive of permanent magnet synchronous motor," *IEEE Access*, vol. 9, pp. 100882–100894, 2021.

[71] R. M. Prasad and M. A. Mulla, "A novel position-sensorless algorithm for field-oriented control of DFIG with reduced current sensors," *IEEE Trans. Sustain. Energy*, vol. 10, no. 3, pp. 1098–1108, 2019.

[72] R. Nair and G. Narayanan, "Stator flux based model reference adaptive observers for sensorless vector control and direct voltage control of doubly-fed induction generator," *IEEE Trans. Ind. Appl.*, vol. 56, no. 4, pp. 3776–3789, 2020.

[73] F. Amrane, A. Chaiba, B. E. Babas, and S. Mekhilef, "Design and implementation of high performance field oriented control for grid-connected doubly fed induction generator via hysteresis rotor current controller," *Rev. Sci. Technol. – Électrotechnique et Énergie*, vol. 61, no. 4, pp. 319–324, 2016.

[74] A. Fayssal, F. Bruno, and C. Azeddine, "Experimental investigation of efficient and simple wind-turbine based on DFIG-direct power control using LCL-filter for stand-alone mode," *ISA Trans.*, vol. 125, pp. 631–664, 2022.

[75] S. Khadar, H. Abu-Rub, and A. Kouzou, "Sensorless field-oriented control for open-end winding five-phase induction motor with parameters estimation," *IEEE Open J. Ind. Electron. Soc.*, vol. 2, pp. 266–279, 2021.

[76] M. Kamarzarrin, M. H. Refan, P. Amiri, and A. Dameshghi, "Fault diagnosis of wind turbine doubly-fed induction generator based on multi-level fusion and measurement of back-to-back converter current signal," *Iran. J. Electr. Electron. Eng.*, vol. 18, no. 2, p. 2074, 2022.

[77] A. B. Moreira, T. A. D. S. Barros, V. S. D. C. Teixeira, R. R. D. Souza, M. V. D. Paula, and E. R. Filho, "Control of powers for wind power generation and grid current harmonics filtering from doubly fed induction generator: comparison of two strategies," *IEEE Access*, vol. 7, pp. 32703–32713, 2019.

[78] Y. Quan, L. Hang, Y. He, and Y. Zhang, "Multi-resonant-based sliding mode control of DFIG-based wind system under unbalanced and harmonic network conditions," *Appl. Sci.*, vol. 9, no. 6, p. 1124, 2019.

[79] I. Yaichi, A. Semmah, P. Wira, and Y. Djeriri, "Super-twisting sliding mode control of a doubly-fed induction generator based on the SVM strategy," *Period. Polytech. Electr. Eng. Comput. Sci.*, vol. 63, no. 3, pp. 178-190, 2019.

[80] M. Said, A. Derouich, N. El Ouanjli, and M. El Mahfoud, "Enhancement of the direct torque control by using artificial neuron network for a doubly fed induction motor," *Intell. Syst. Appl.*, vol. 13, pp. 1–18, 2022.

[81] M. M. Alhato and S. Bouallègue, "Direct power control optimization for doubly fed induction generator based wind turbine systems," *Math. Comput. Appl.*, vol. 24, no. 3, p. 77, 2019.

[82] N. A. Yusoff, A. M. Razali, K. A. Karim, T. Sutikno, and A. Jidin, "A concept of virtual-flux direct power control of three-phase AC-DC converter," *Int. J. Power Electron. Drive Syst.*, vol. 8, no. 4, pp. 1776–1784, 2017.

[83] A. Yahdou, B. Hemici, and Z. Boudjema, "Second order sliding mode control of a dual-rotor wind turbine system by employing a matrix converter," *J. Electr. Eng.*, vol. 16, pp. 1–11, 2016.

[84] E. Najib, D. Aziz, E. Abdelaziz, T. Mohammed, E. Youness, M. Khalid, and B. Badre, "Direct torque control of doubly fed induction motor using three-level NPC inverter," *Prot. Control Mod. Power Syst.*, vol. 4, no. 17, pp. 1–9, 2019.

[85] C. Hamid, D. Aziz, C. Seif Eddine, Z. Othmane, T. Mohammed, and E. Hasnae, "Integral sliding mode control for DFIG based WECS with MPPT based on artificial neural network under a real wind profile," *Energy Rep.*, vol. 7, pp. 4809–4824, 2021.

[86] H. Ravikiran and M. Tukaram, "Modified super twisting algorithm based sliding mode control for LVRT enhancement of DFIG driven wind system," *Energy Rep.*, vol. 8, pp. 3600–3613, 2022.

[87] Y. Ibrahim, A. Semmah, and P. Wira, "Neuro-second order sliding mode control of a DFIG based wind turbine system," *J. Electr. Electron. Eng.*, vol. 13, no. 1, pp. 63–68, 2020.